Observing the gamma diffuse emission

Molecular Clouds in gamma rays

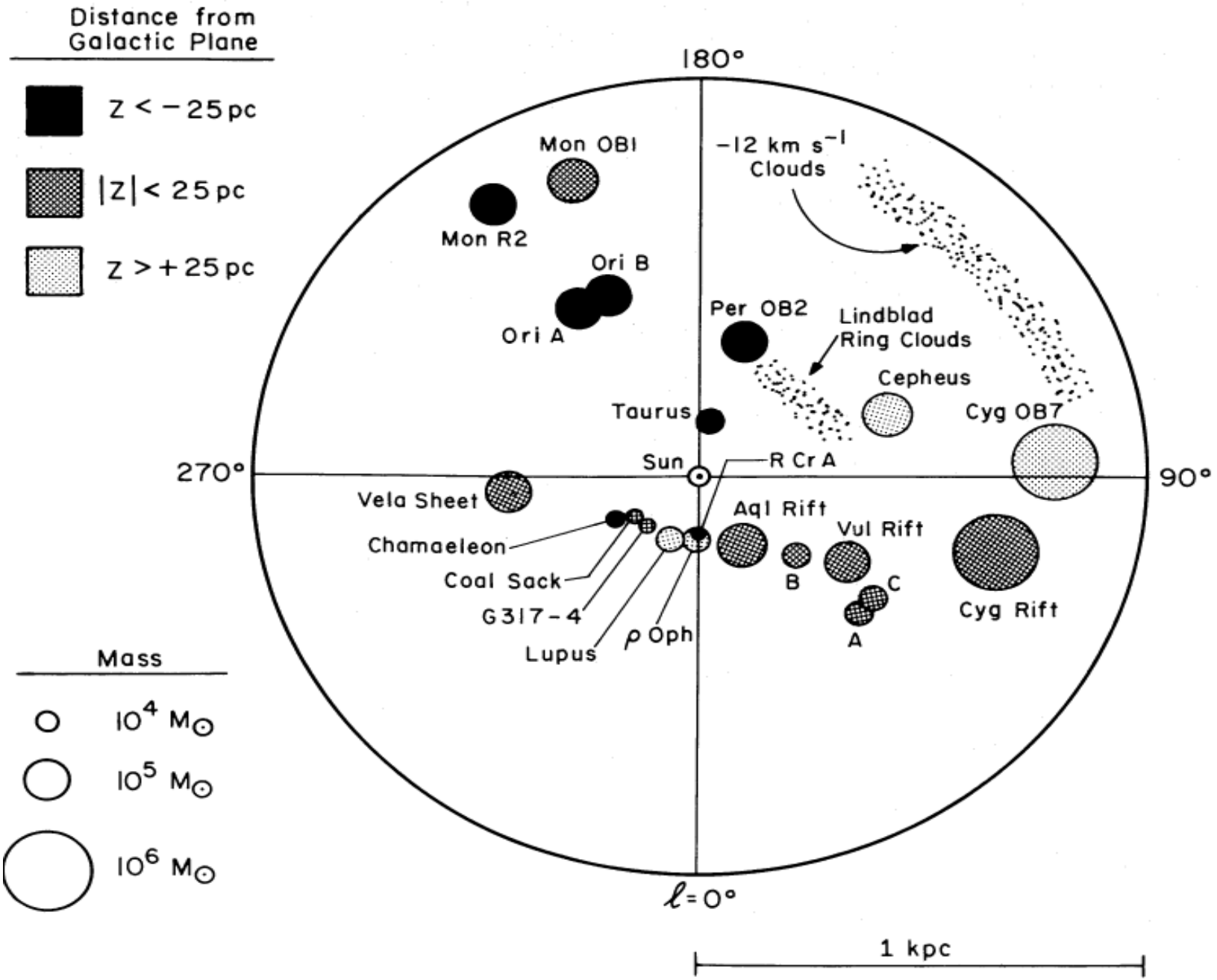

Molecular Clouds in gamma rays

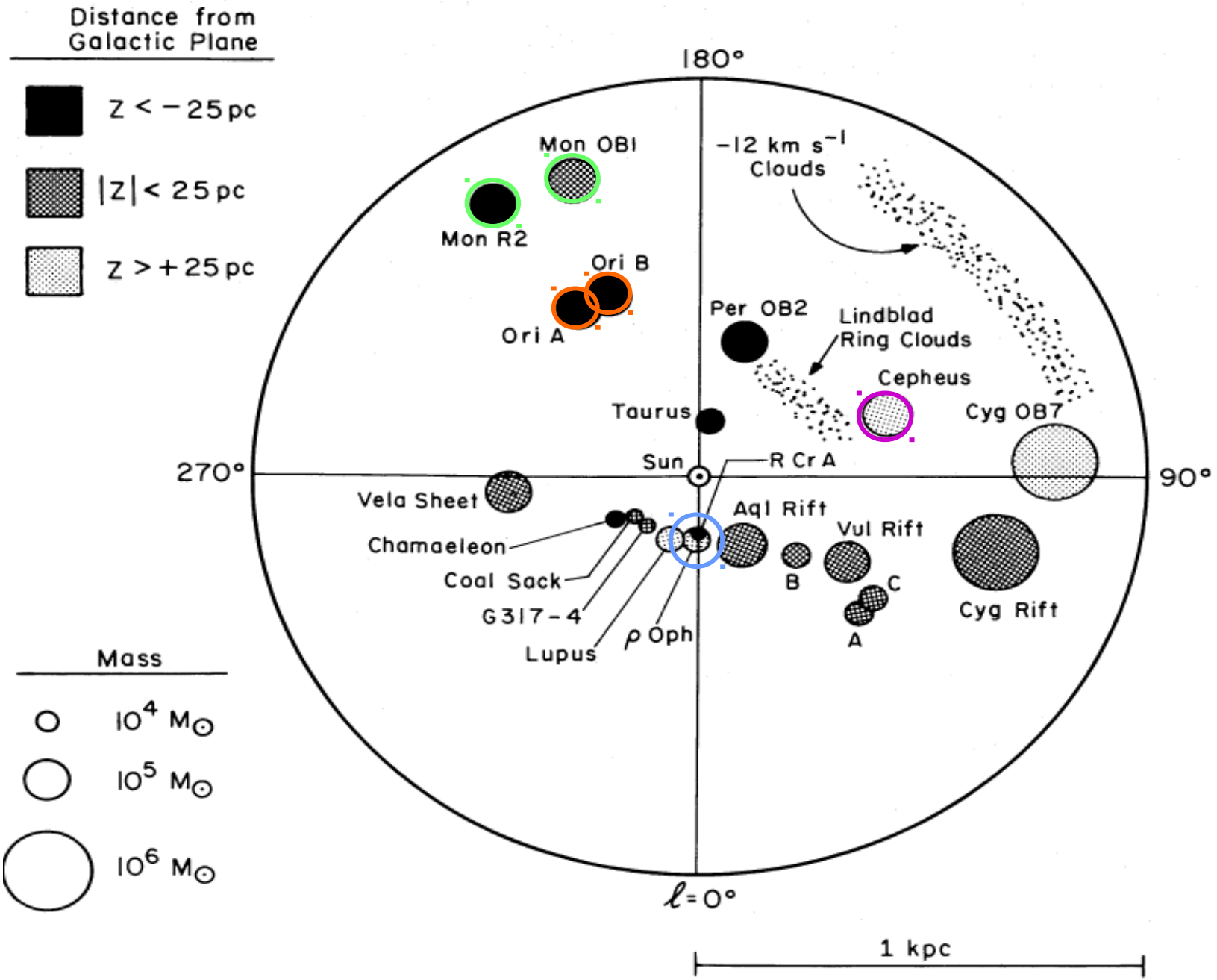

Molecular Clouds in gamma rays

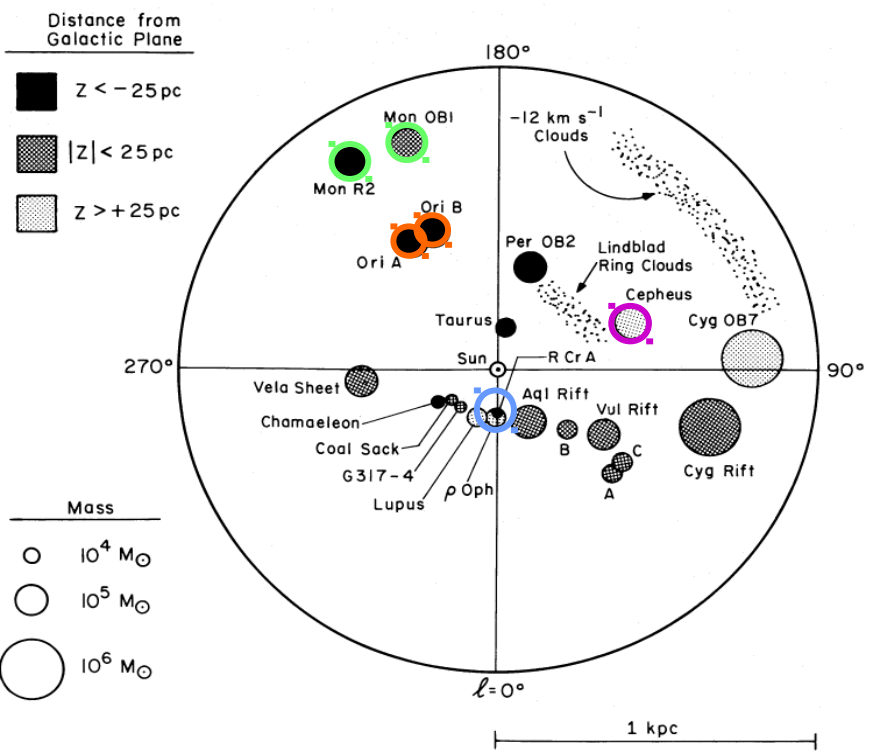

Digel et al. (1996 & 2001)

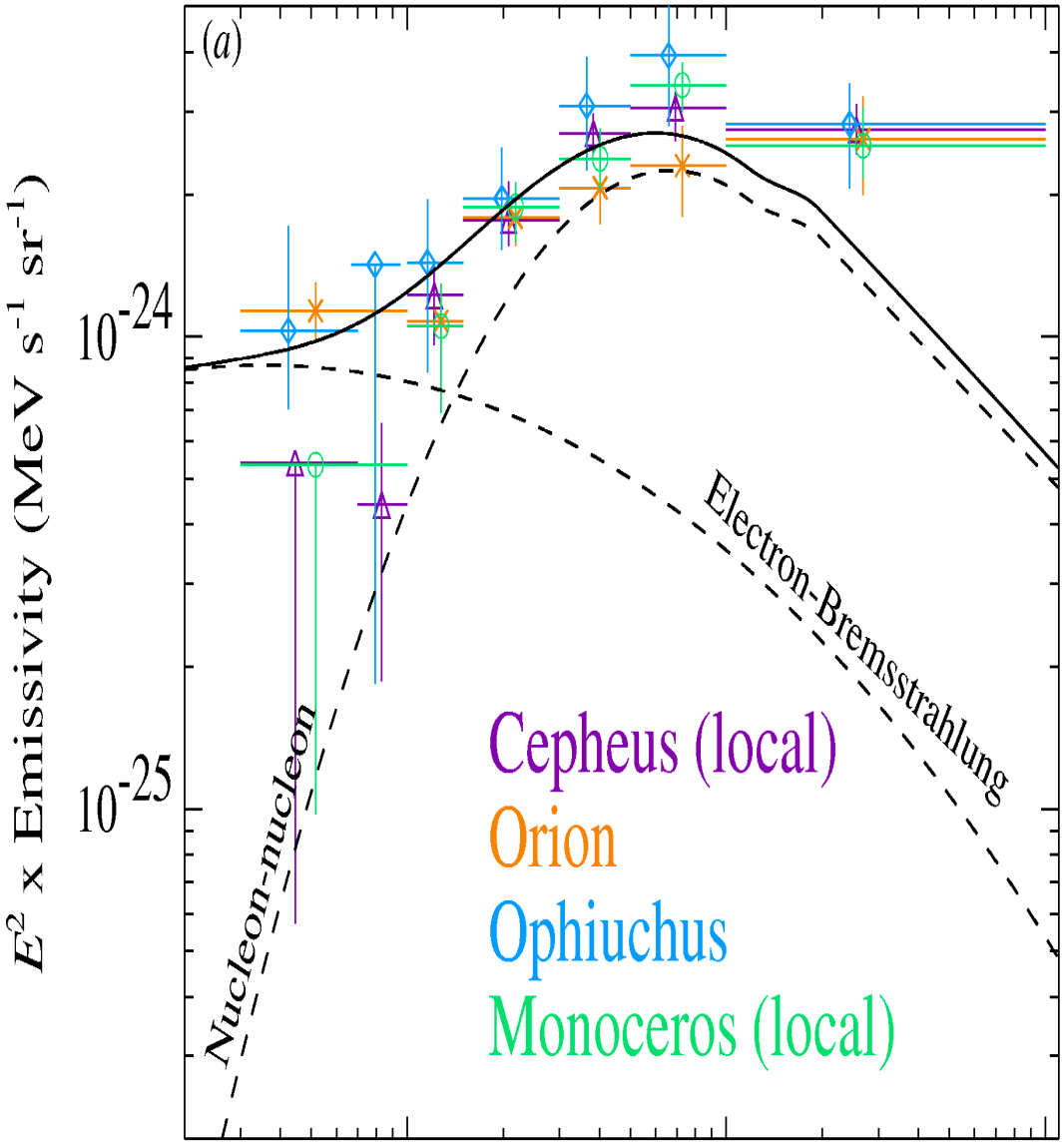

W 28

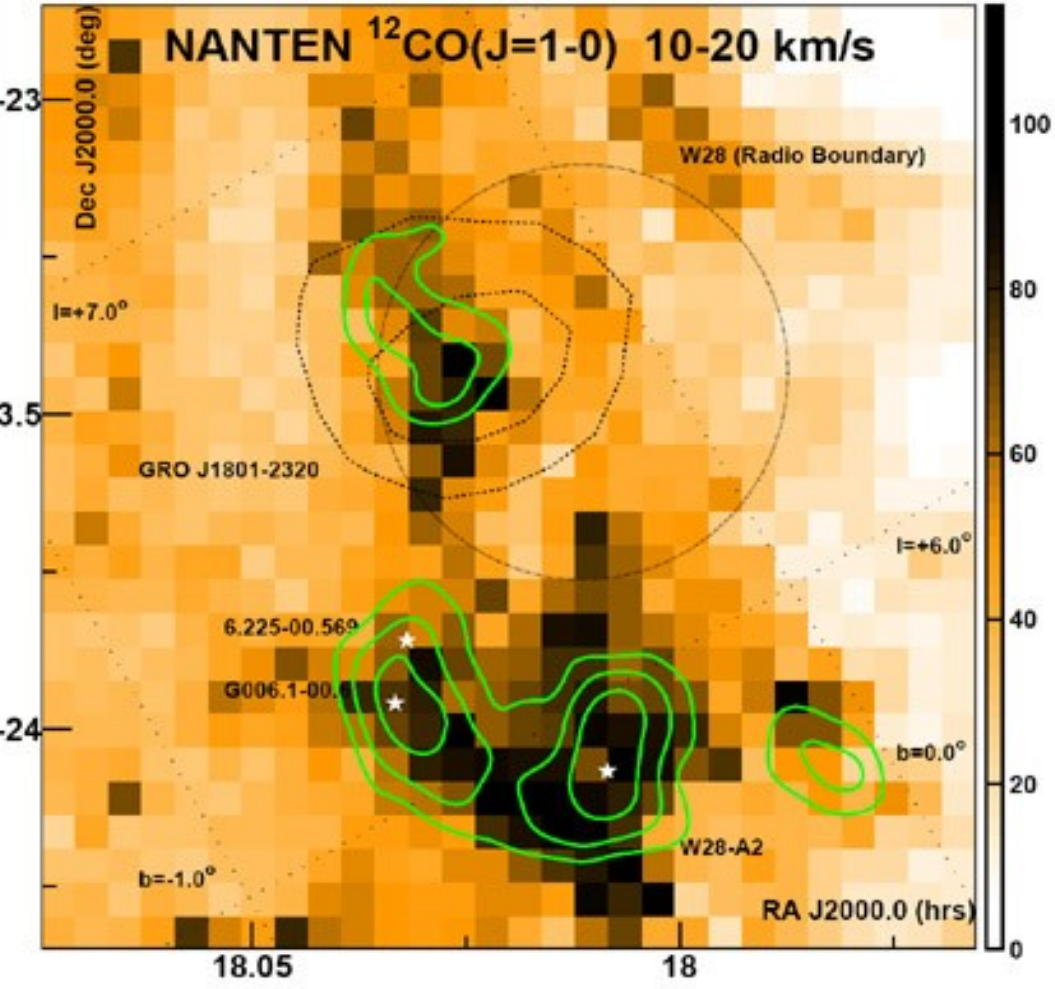
NANTEN ^{12}CO(J=1-0) 10-20 km/s
W28 (Radio Boundary)
GRO J1801-2320
l=+7.0°
l=+6.0°
6.225-00.56°
G006.1-00.6
b=0.0°
W28-A2
b=-1.0°
Dec J2000.0 (deg)
RA J2000.0 (hrs)
-23
-24
18.05
18
100
80
60
40
20
0

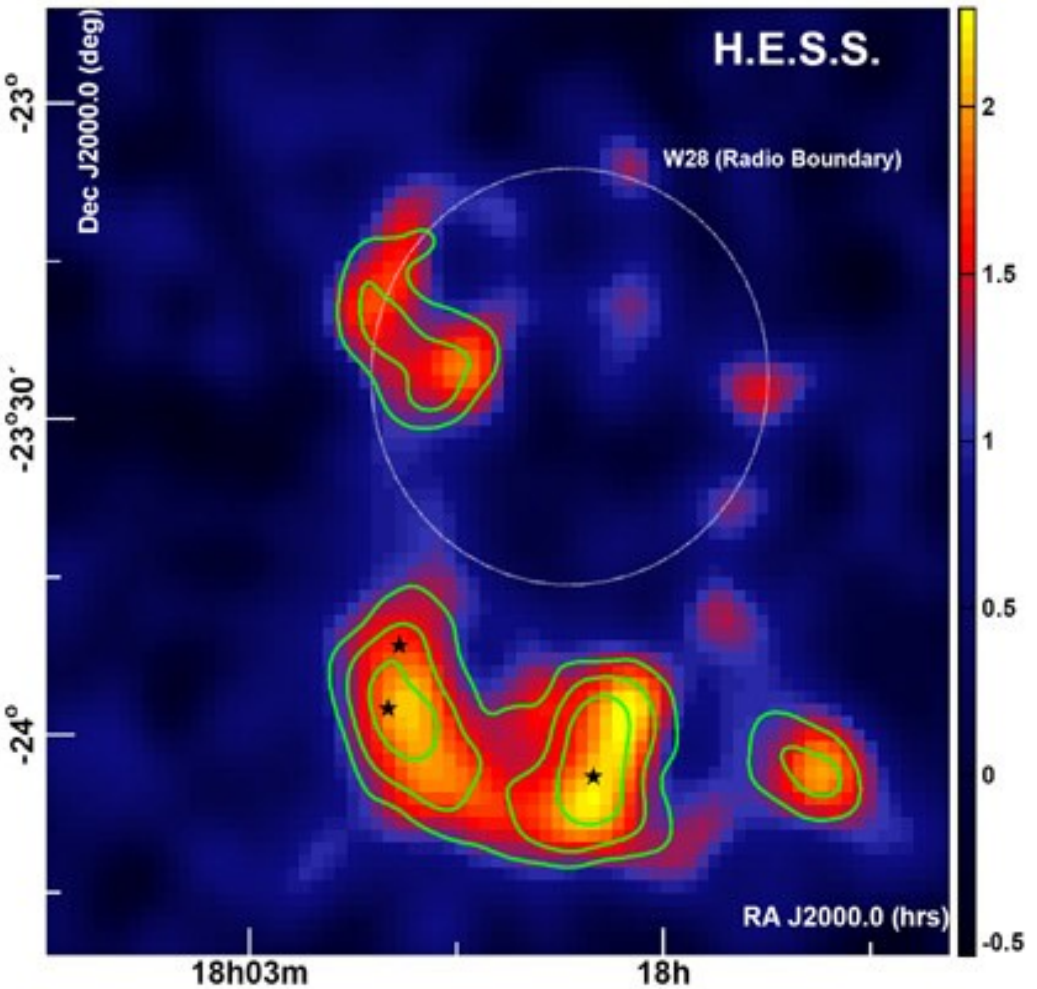
H.E.S.S.
W28 (Radio Boundary)
Dec J2000.0 (deg)
RA J2000.0 (hrs)
-23°
-23°30′
-24°
18h03m
18h
2
1.5
1
0.5
0
-0.5

W 28

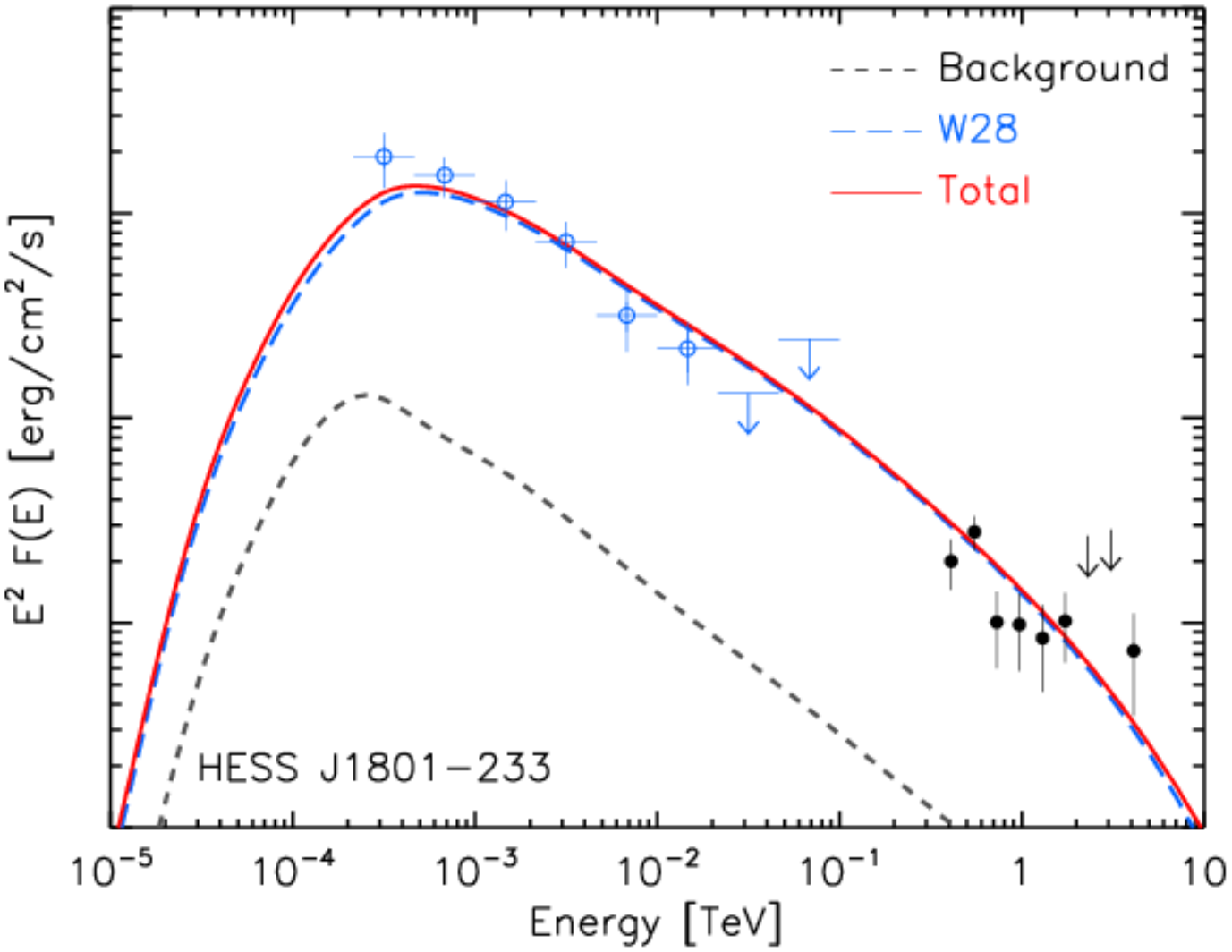

D = 3 kpc

F = 1.1 10^{-6} ph / cm^2 s

From gamma rays to CR

CR distribution

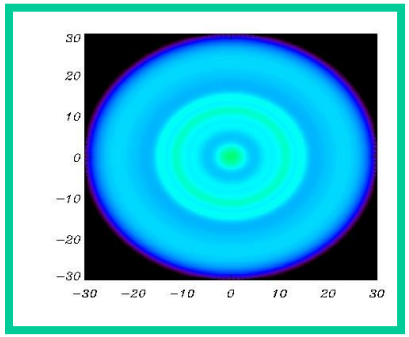

Targets distribution

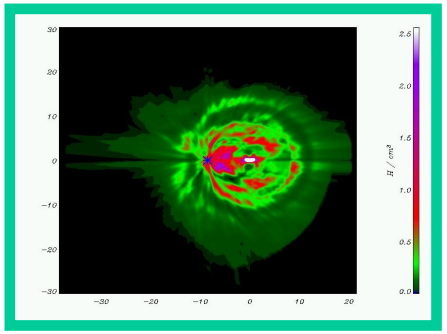

$\int$ Along the line of sight

Gamma Ray Data

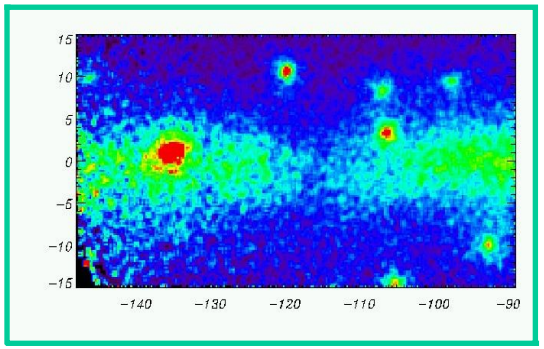

Gamma Ray model

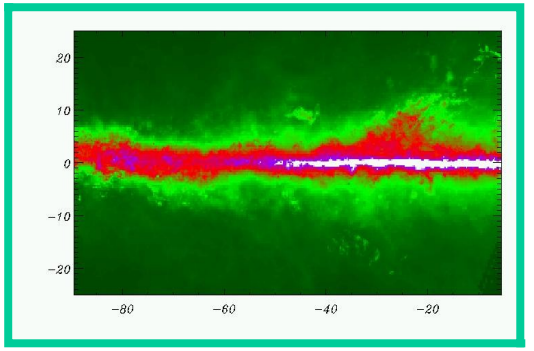

The γ-ray emission model (II quadrant)

HI

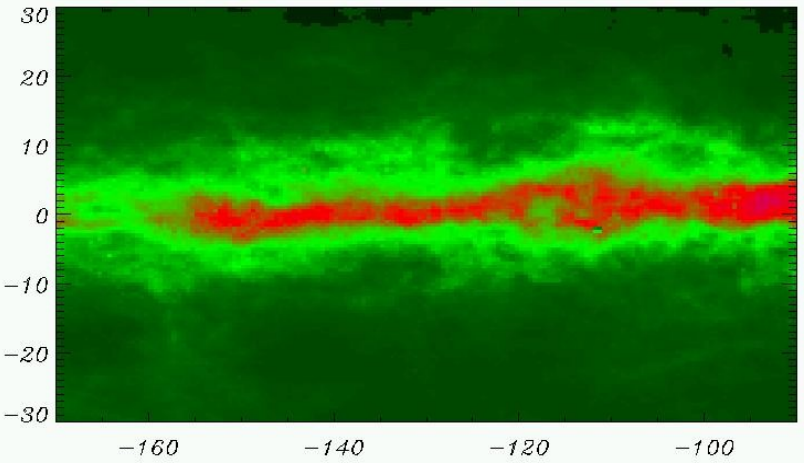

H2

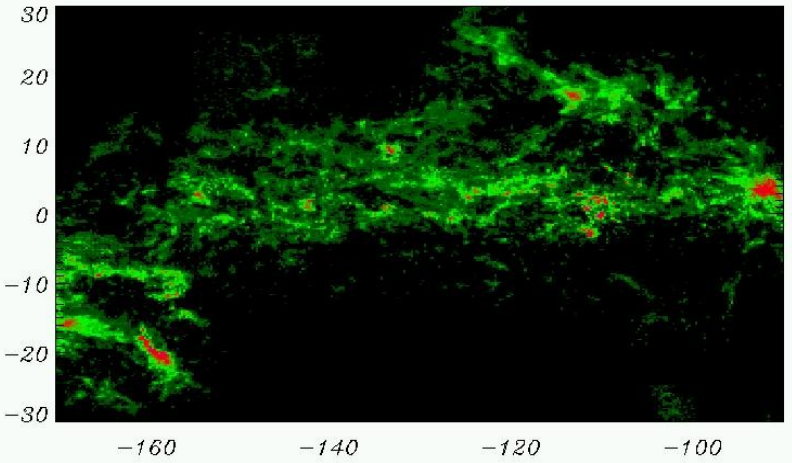

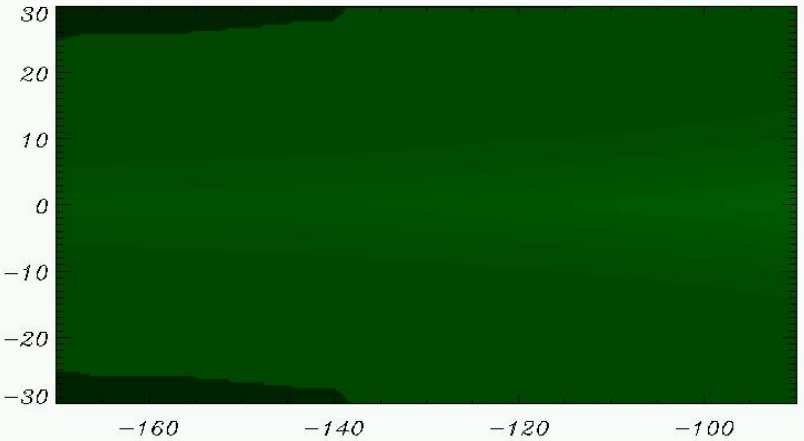

ISRF

The γ-ray emission model (II quadrant)

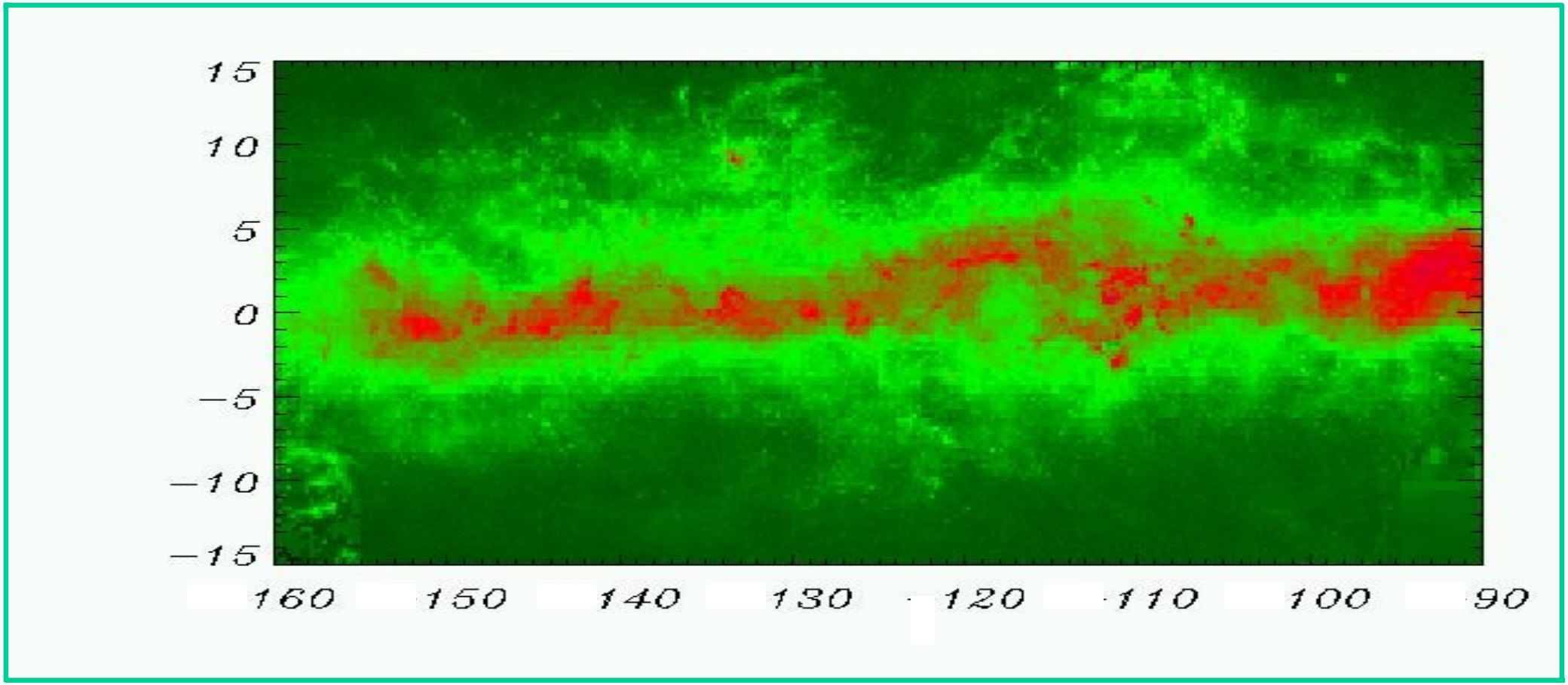

Model vs. Observations

(II quadrant)

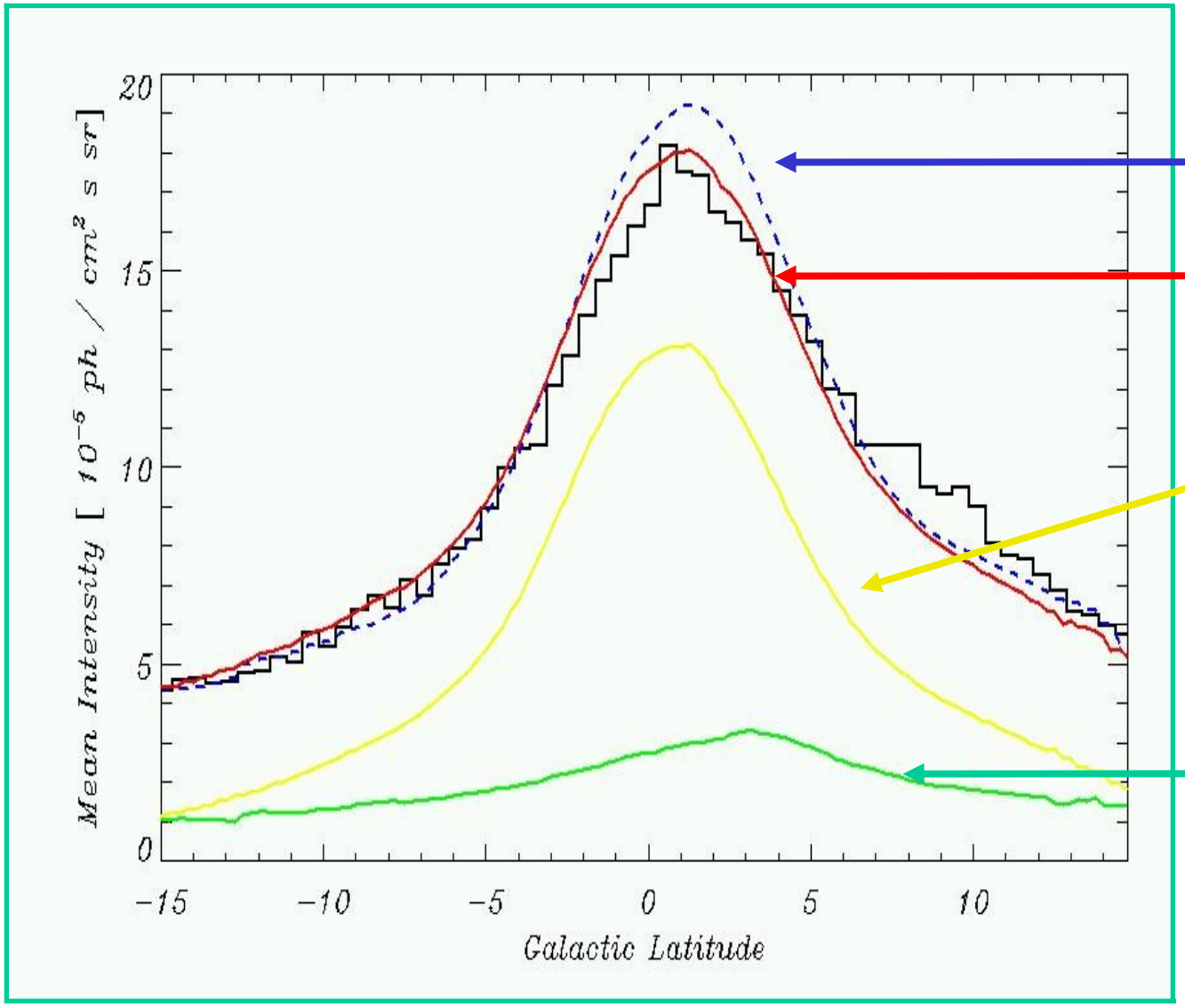

EG. model

AG. model

Emission from HI regions

Emission from molecular clouds

Model vs. Observations

(II quadrant)

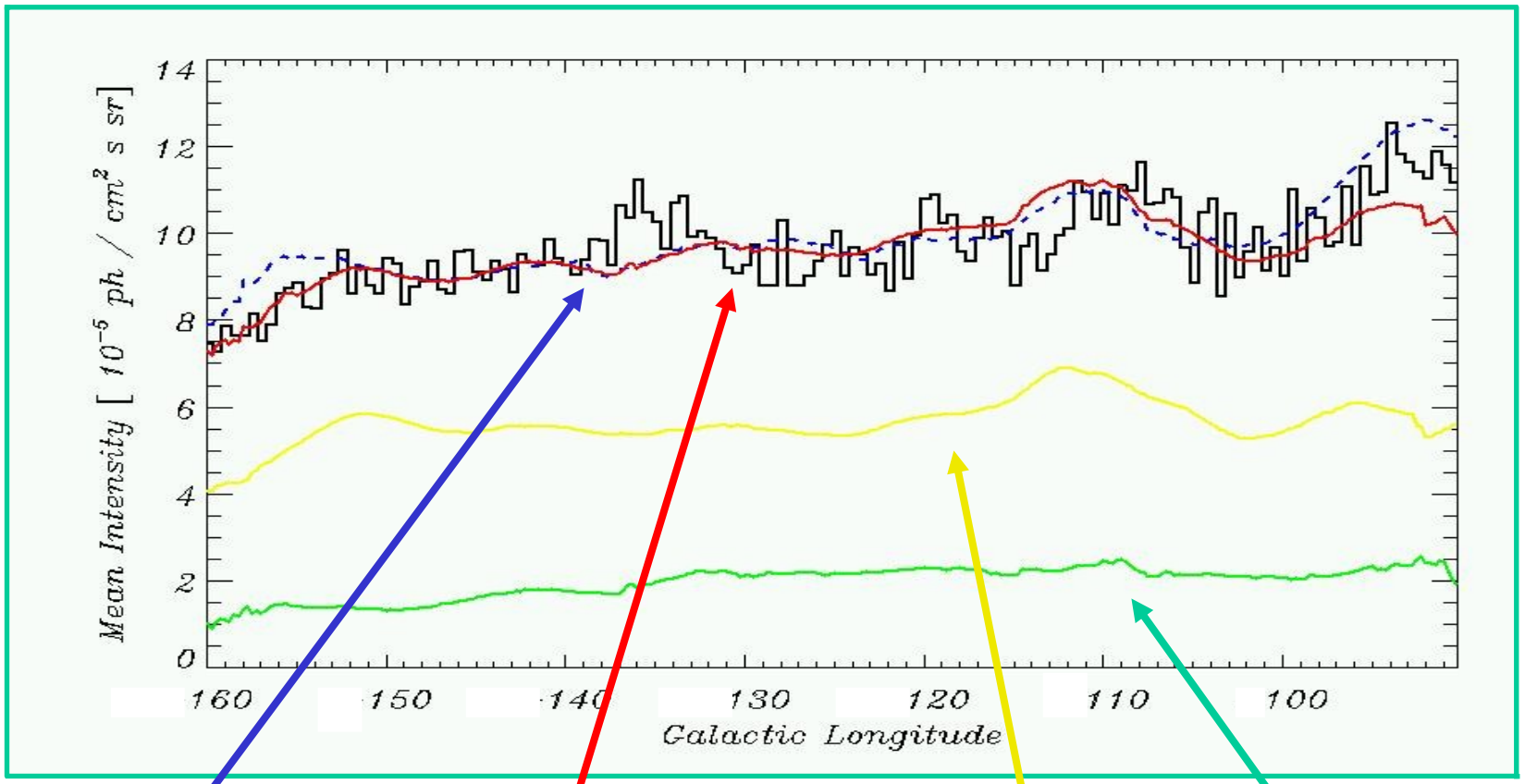

EG. model

AG. model

Emission from HI regions

Emission from molecular clouds

Gamma-Ray Spectrum

$$S(E)=\frac{1}{4\pi}\int\left[q_{pp}(r,E)\,n(r)+q_{br}(r,E)\,n(r)+q_{IC}(r,E)\,U(r)\right]dr\,d\Omega$$

Electron Bremsstrahlung

π^{o} decay

Inverse Compton

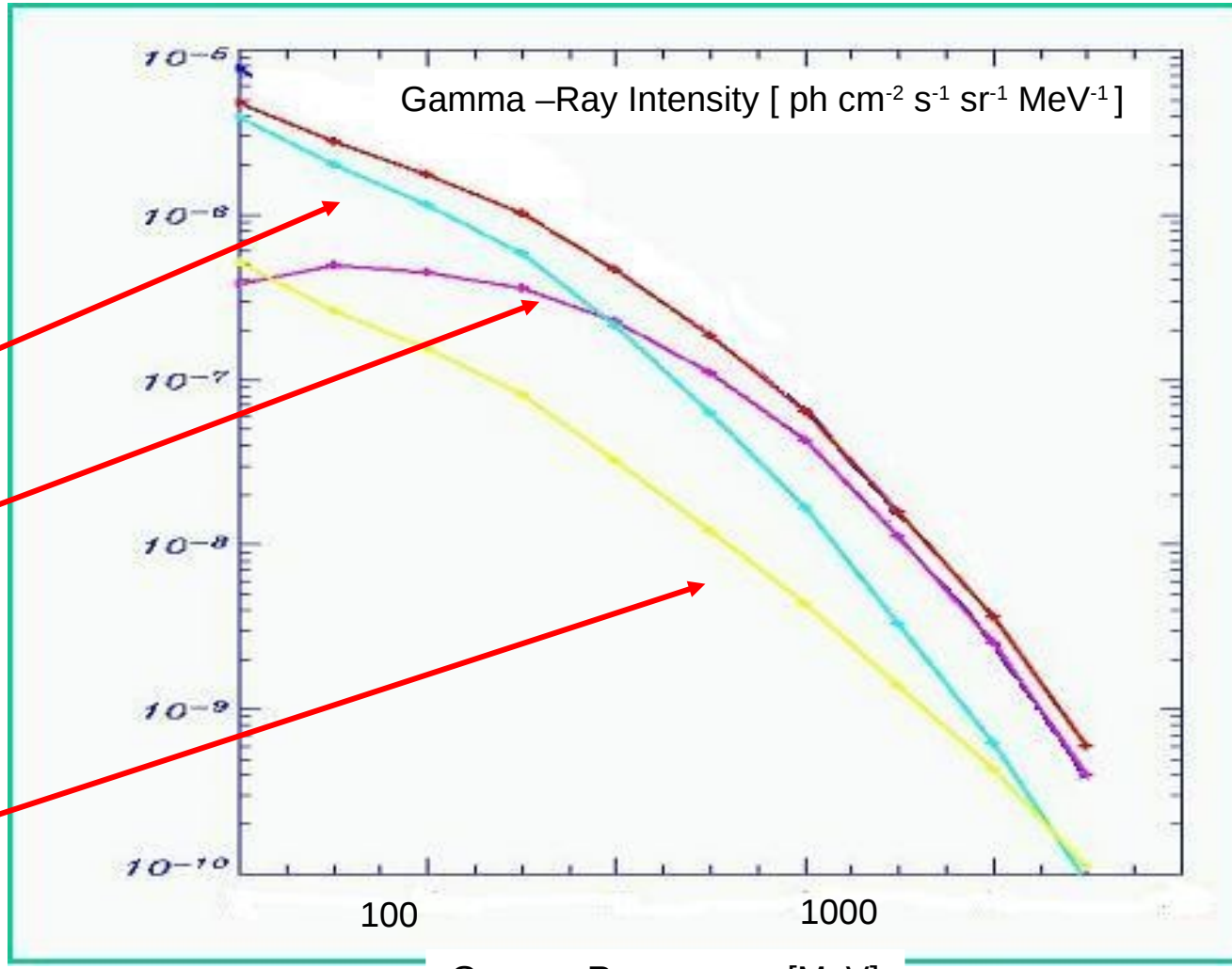

Results from EGRET

π^0 bump in the inner Milky Way
(Hunter et al. 1997)

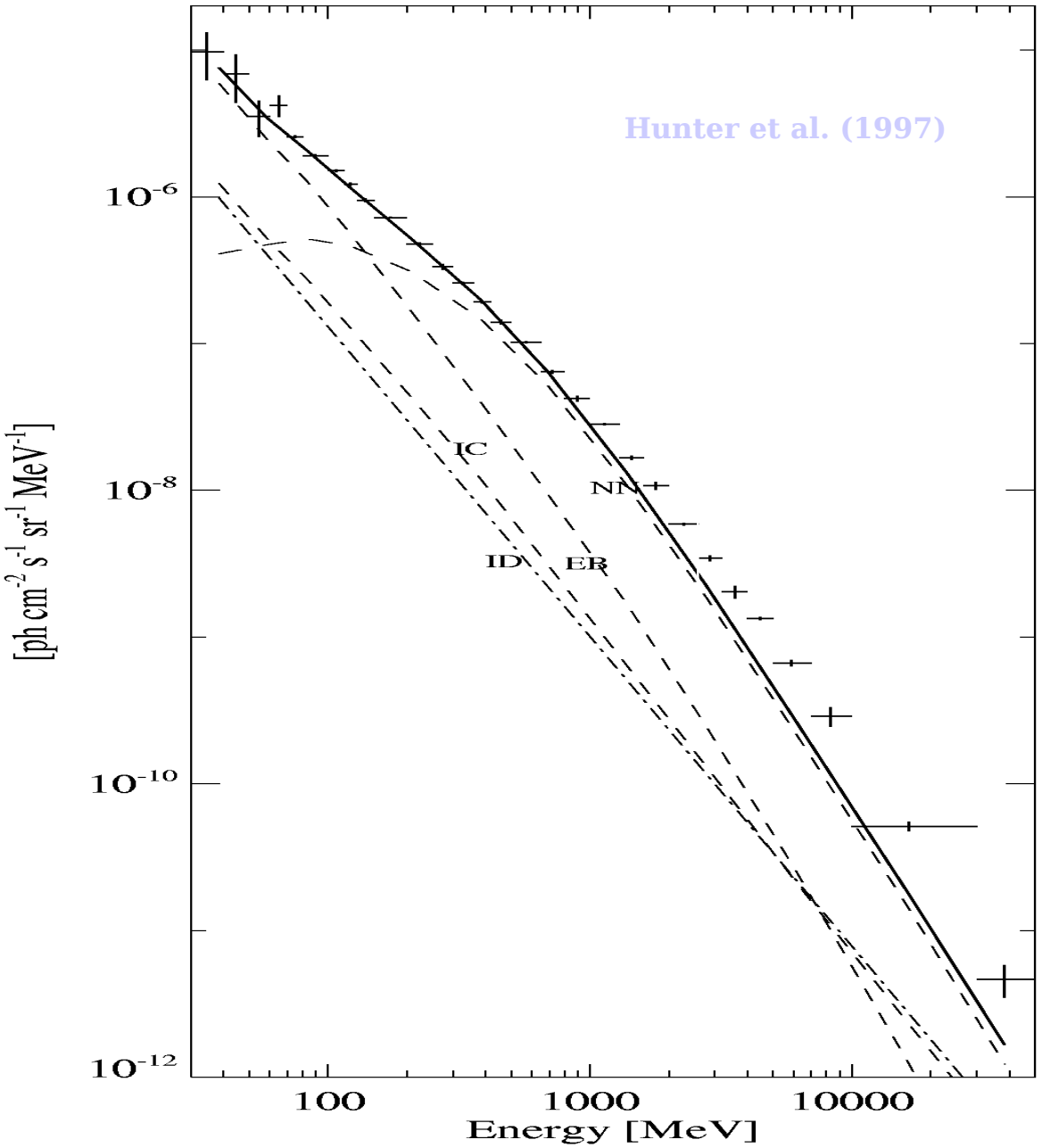

Results from EGRET

Spatial correlation between gaz and γ-rays

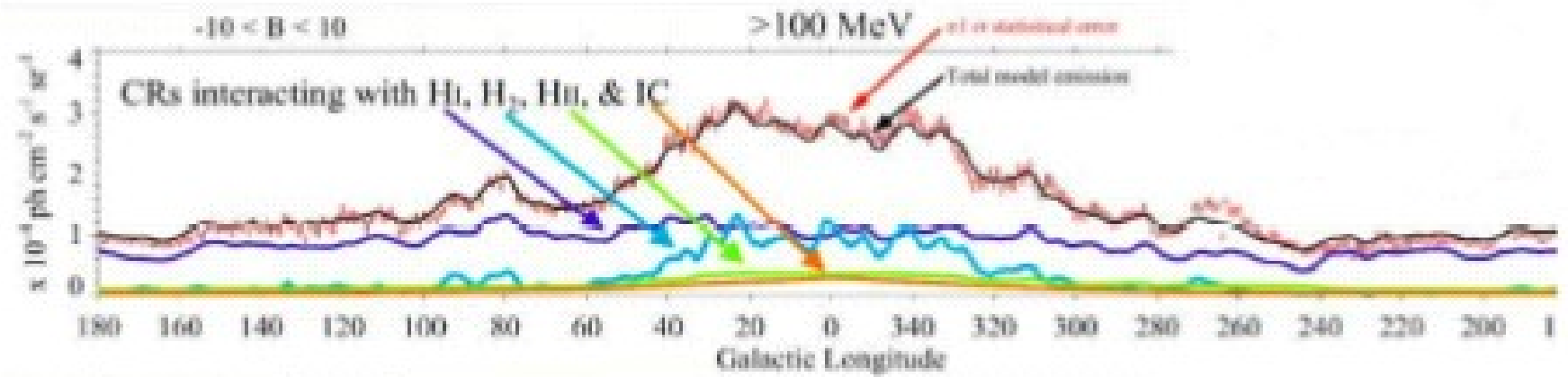

Observations (EGRET):

- large scale spatial distribution well modelled by combination of ISM phases (assuming $I \propto \rho^2$)
- fraction of unresolved point sources is small (unless distributed like the interstellar gas)
- spectrum does not vary (within relatively small uncertainties) in the Galaxy
- deviations from perfect fit

Implications:

- Gamma-Rays probe galactic CR and ISM distributions
- CR electron-to-proton ratio roughly constant throughout Galaxy
- assumption of dynamic balance ($I \propto \rho^2$) between ISM and CR is reasonably correct
  (large matter density implies larger magnetic fields, allowing for larger CR energy density)

CRs in Molecular Clouds

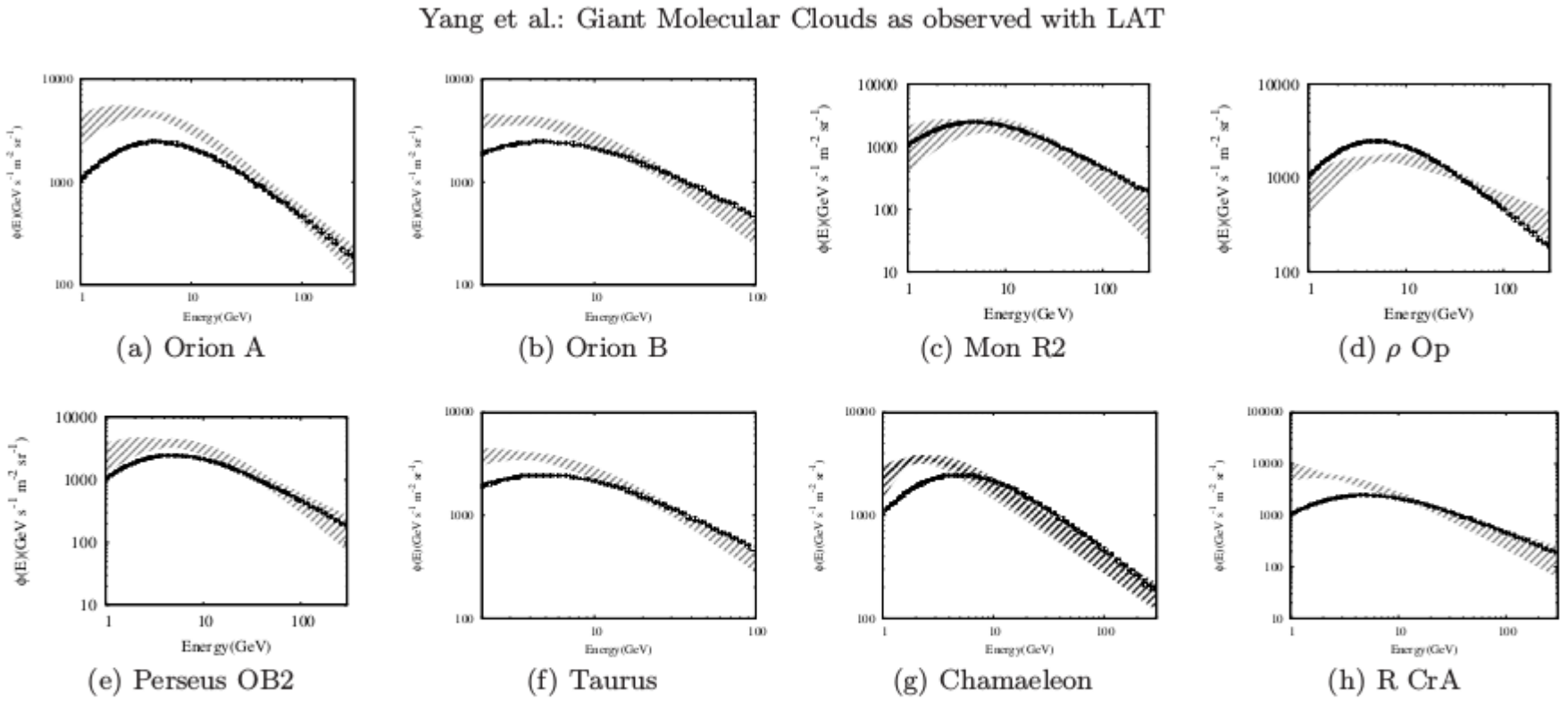

Fig. 5. Energy spectra of CR protons in different clouds derived from the γ-ray data. It is assumed that the interactions of CR with the ambient gas are fully responsible for the observed γ-ray fluxes. The shaded regions represent 1σ fits for the proton spectra. For comparison, the measurements of CR protons by PAMELA are also shown (black crosses).

CRs in Molecular Clouds

Yang et al.: Giant Molecular Clouds as observed with LAT

Table 2. Spectral characteristics and statistic test (TS) value of the GMC listed in Table 1 obtained from the LAT data. The individual χ^2/d.o.f. of the spectral representation tested are also quoted with the corresponding probabilities in brackets (see text for more details).

#	Region	TS	Flux at 3 GeV $[10^{-9}\mathrm{GeV}^{-1}\mathrm{cm}^{-2}\mathrm{s}^{-1}$	E_b [GeV]	^{2}/d.o.f. (BPL)	χ^2/d.o.f. (KPL)	χ^2/d.o.f. (TPL)
1	ρ Oph	11648	7.7 ± 0.8	4.7 ± 2.3	10.7/9 (0.30)	22.2/11 (0.024)	13.9/11 (0.24)
2	Orion B	6107	3.0 ± 0.6	3.6 ± 1.3	10.8/9 (0.29)	27.9/11 (2.3×10^{-3})	13.1/11 (0.29)
3	Orion A	22021	5.9 ± 0.7	4.3 ± 1.2	11.0/10 (0.35)	40.1/12 (4.9×10^{-5})	14.0/12 (0.30)
4	Mon R2	1607	1.3 ± 0.2	3.0 ± 0.7	10.5/10 (0.39)	29.4/12 (3.4×10^{-3})	13.4/12 (0.34)
5	Taurus	5670	9.8 ± 1.5	4.7 ± 1.5	10.5/10 (0.39)	36.9/12 (2.3×10^{-4})	16.5/12 (0.17)
6	R CrA	2315	1.2 ± 0.8	0.9 ± 0.8	5.1/9 (0.82)	7.4/11 (0.76)	15.0/11 (0.18)
7	Chamaeleon	2917	2.0 ± 0.5	2.0 ± 0.9	9.2/9 (0.42)	24.0/11 (0.01)	12.0/11 (0.36)
8	Perseus OB2	6410	3.8 ± 0.3	4.9 ± 2.1	11.7/10 (0.30)	20.8/12 (0.05)	17.3/12 (0.14)

W 28

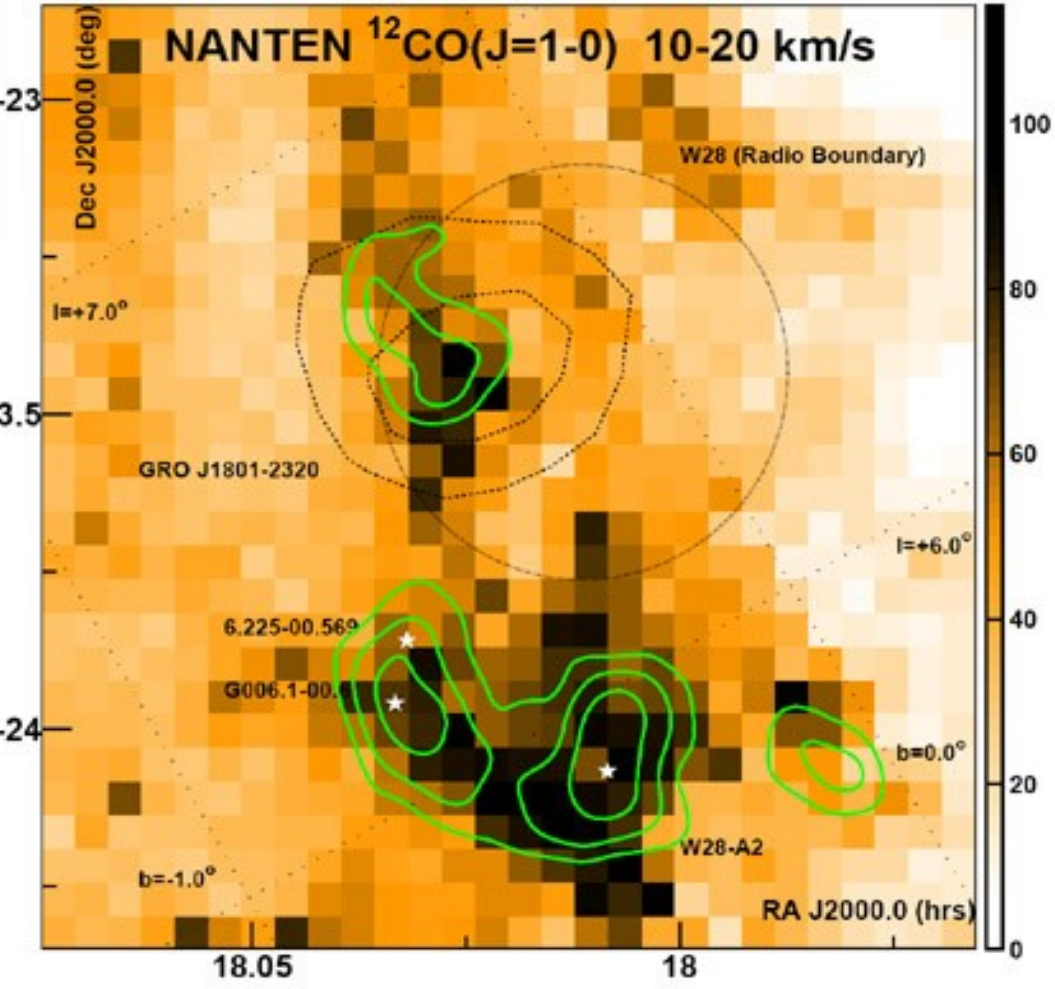
NANTEN ^{12}CO(J=1-0) 10-20 km/s
W28 (Radio Boundary)
GRO J1801-2320
l=+7.0°
l=+6.0°
6.225-00.56°
G006.1-00.6
b=0.0°
W28-A2
b=-1.0°
Dec J2000.0 (deg)
RA J2000.0 (hrs)
-23
-24
18.05
18
100
80
60
40
20
0

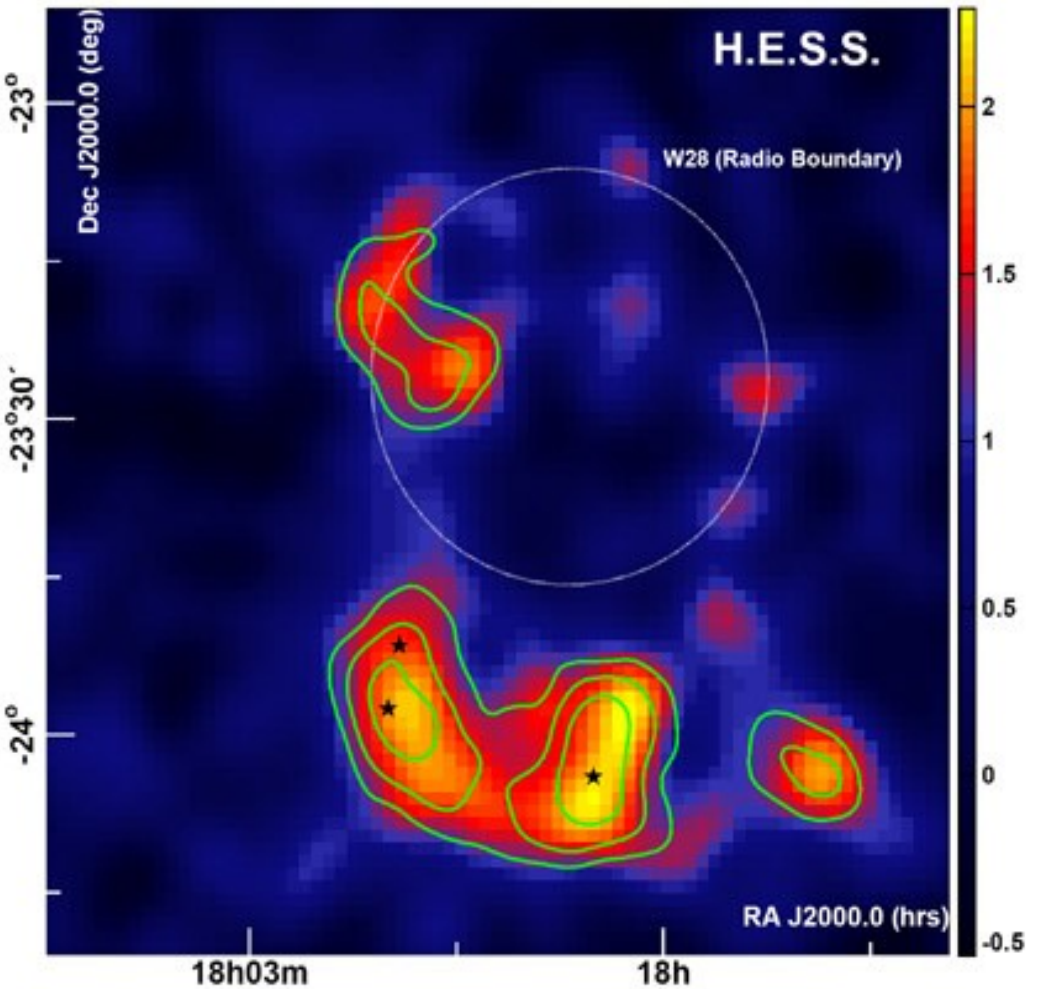
H.E.S.S.
W28 (Radio Boundary)
Dec J2000.0 (deg)
RA J2000.0 (hrs)
-23°
-23°30′
-24°
18h03m
18h
2
1.5
1
0.5
0
-0.5

W 28

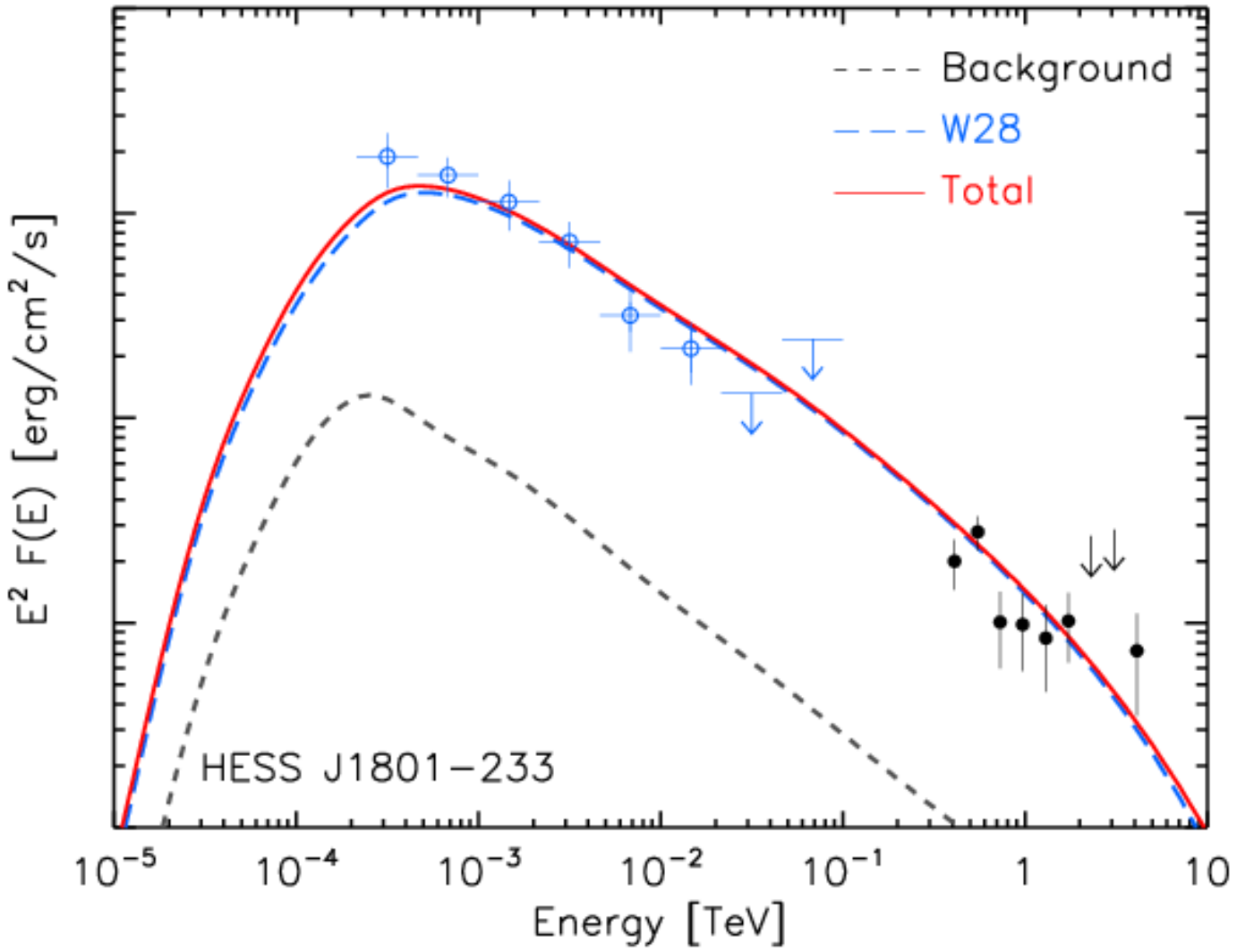

D = 3 kpc

F = 1.1 10^{-6}

ph / cm^2 s

Gamma rays from stars

As presented in Fig 2, for a given point x on the line-of-

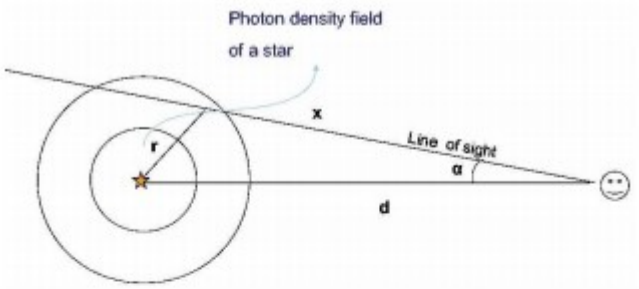

Fig. 2 Definition of variables for eq (3).

sight, the surface photon density is proportional to $1/r^2$, where $r^2 = x^2 + d^2 - 2\,d\,x\,cos\alpha$, with d distance from the star. Integrating the photon density over the line of sight from $x = 0$ to $x = \infty$ and over the solid angle, the total photon flux produced by inverse Compton becomes:

$$f(E_\gamma) = \frac{1}{4\pi}\int_0^{2\pi} d\varphi \int_0^{\alpha} sin\alpha\; d\alpha \int dE_{ph}$$
$$\times \int \sigma_{KN}(\gamma, E_{ph}, E_\gamma)\; c\; N(E_e)\; dE_e\; \frac{n_{ph}(R)}{4}\; R^2$$
$$\times \int_0^{\infty} \frac{dx}{x^2 + d^2 - 2\;x\;d\;cos\alpha} =$$
$$= \frac{R^2}{16d}(\pi\alpha + (\frac{\pi}{2})^2 - arctan^2(cot\alpha))$$
$$\times \int dE_{ph} \int \sigma_{KN}\; c\; N(E_e)\; n_{ph}(R)\; dE_e \qquad (3)$$

which for small α is proportional to α/d and the intensity I (per solid angle) is proportional to $1/(\alpha d)$.

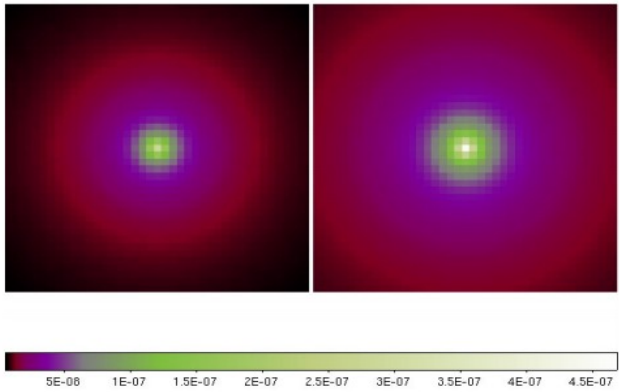

Figure 3: Expected profile of zeta Ori (T_E =30500 K, Radius = 22.1 R_{SUN}) above 100 MeV. On the left the distance is 400 pc taken from [7], on the right the distance is 250 pc [8]. The scale shows the intensity (cm^{-2} s^{-1} sr^{-1}) above 100 MeV. The region shown is 20° wide.

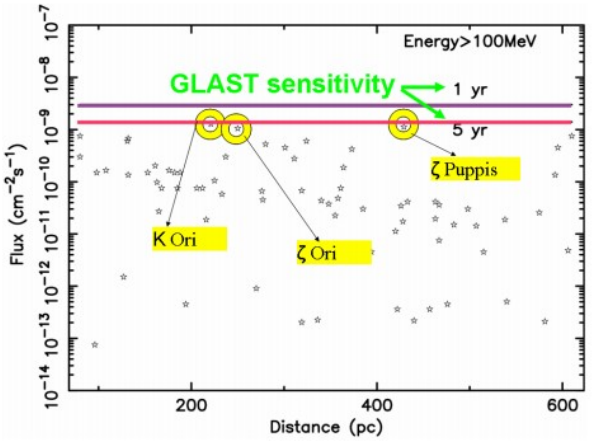

Figure 4: Gamma flux integrated over 5° from the 70 most luminous stars from the Hipparcos catalogue for E > 100 MeV, compared with the GLAST point source sensitivity for 1 and 5 years observations (horizontal lines).

E. Orlando · A. W. Strong

Gamma rays from halos around stars and the Sun

Gamma rays from the Sun

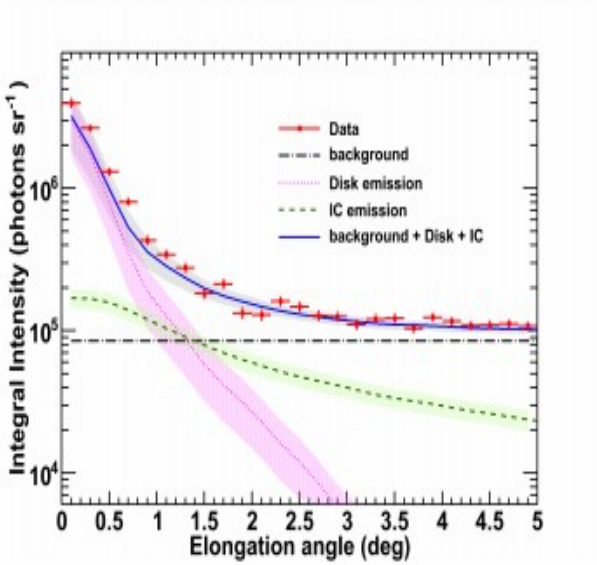

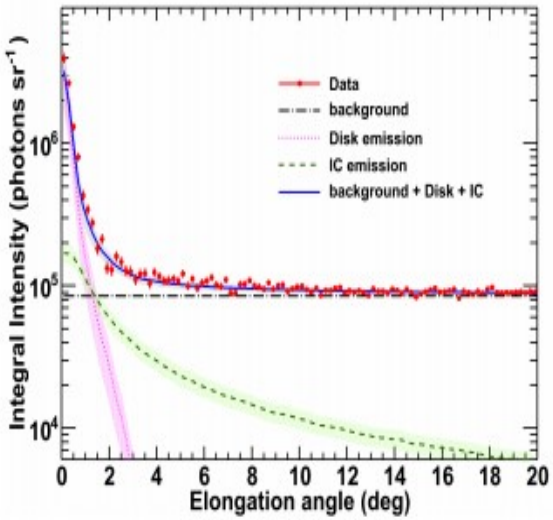

Figure 5. Integral intensity profiles above 500 MeV for elongation angles $\leq 5°$ (top) and $\leq 20°$ (bottom). Points (red) are the observed counts, dash-dotted horizontal (black) line is the background, dotted (magenta) and dashed (green) lines are the point-like and extended components of the emission, correspondingly. The solid (blue) line is the sum of the background and the two components of the emission. The shaded areas around the lines show total error estimates. See text for details.

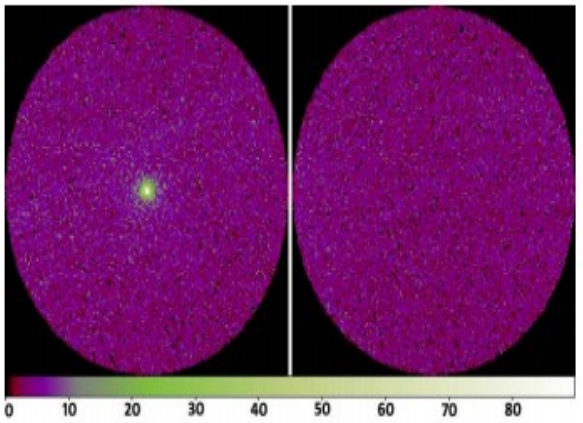

Figure 1. Count maps for events $\geq$100 MeV taken between August 2008 and February 2010 and centered on the Sun (left) and on the trailing source (so-called fake-Sun, right) representing the background. The ROI has $\theta = 20°$ radius and pixel size $0.25° \times 0.25°$. The color bar shows the number of counts per pixel.

Fermi–LAT OBSERVATIONS OF TWO GAMMA-RAY EMISSION COMPONENTS FROM THE QUIESCENT SUN

A. A. ABDO[1], M. ACKERMANN[2], M. AJELLO[2], L. BALDINI[3], J. BALLET[4], G. BARBIELLINI[5,6], D. BASTIERI[7,8], K. BECHTOL[2]

..from the Earth atmosphere

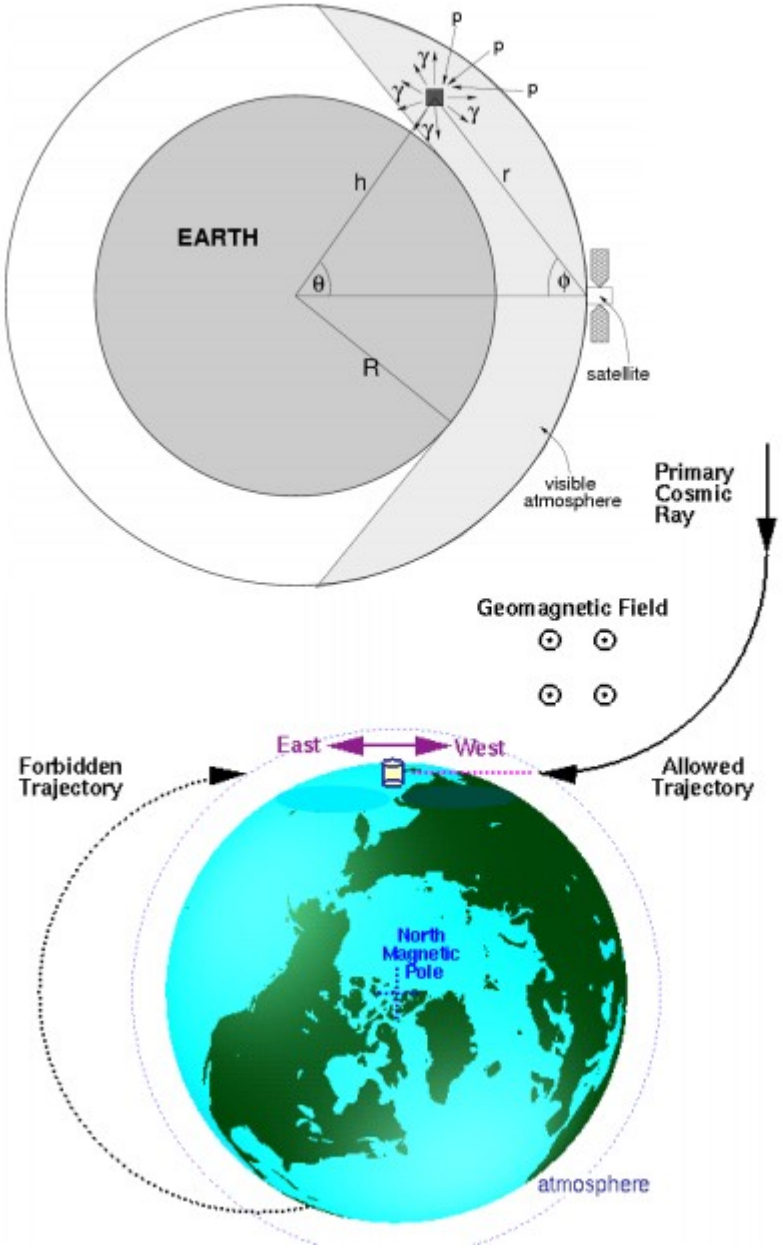

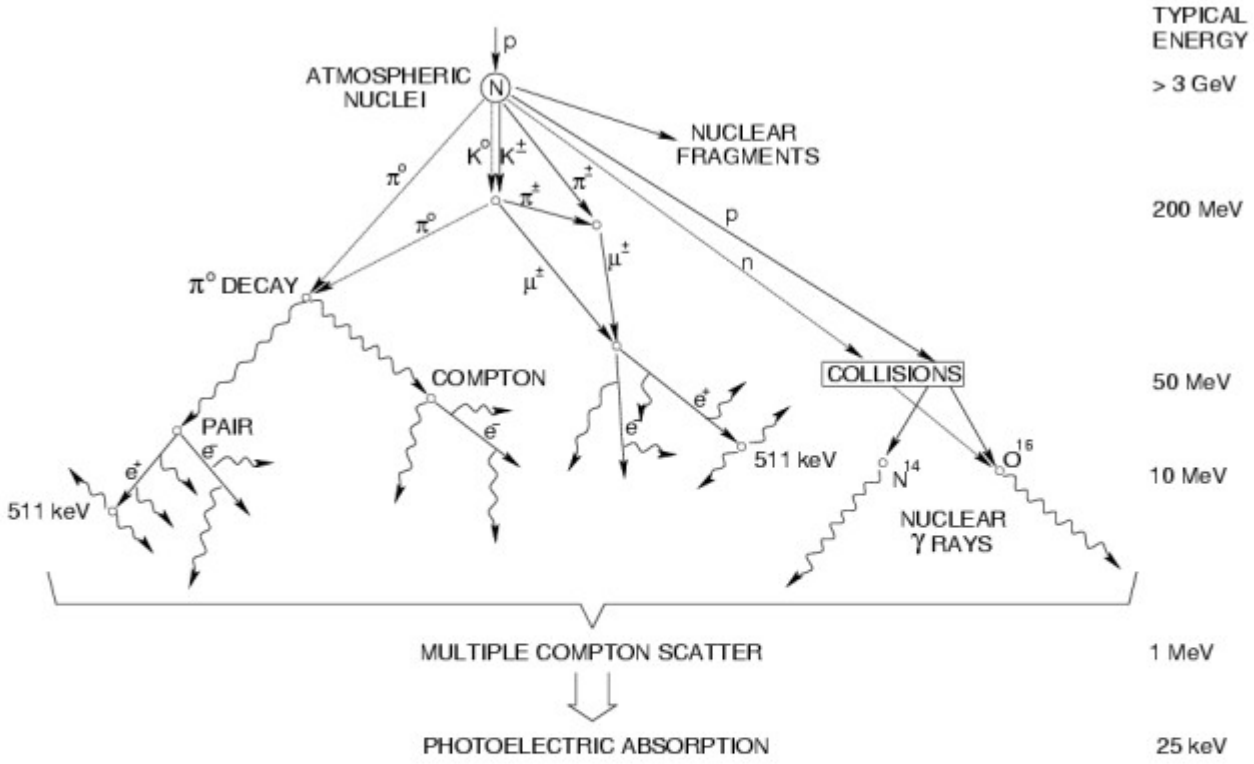

Diagrams taken from:
- Shaw S. E., et al. 2003, A&A, 398, 391-402
- http://hep.bu.edu/~superk/ew-effect.html

..from the Earth atmosphere

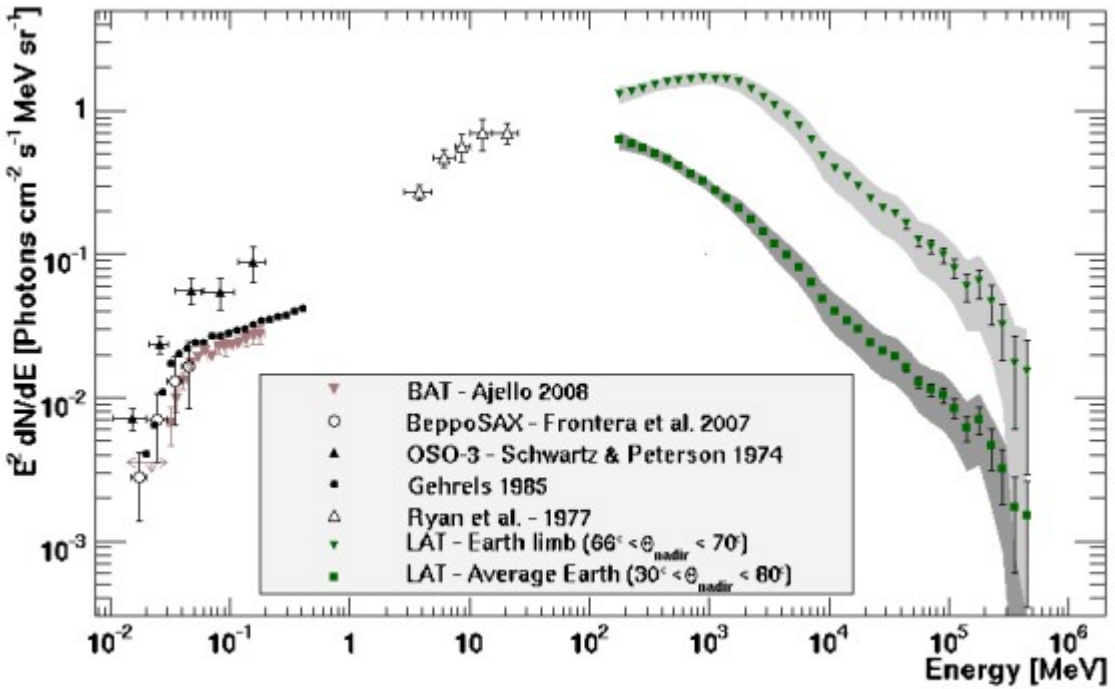

Flux Maps

East-West effect clearly visible, getting smaller at higher energy

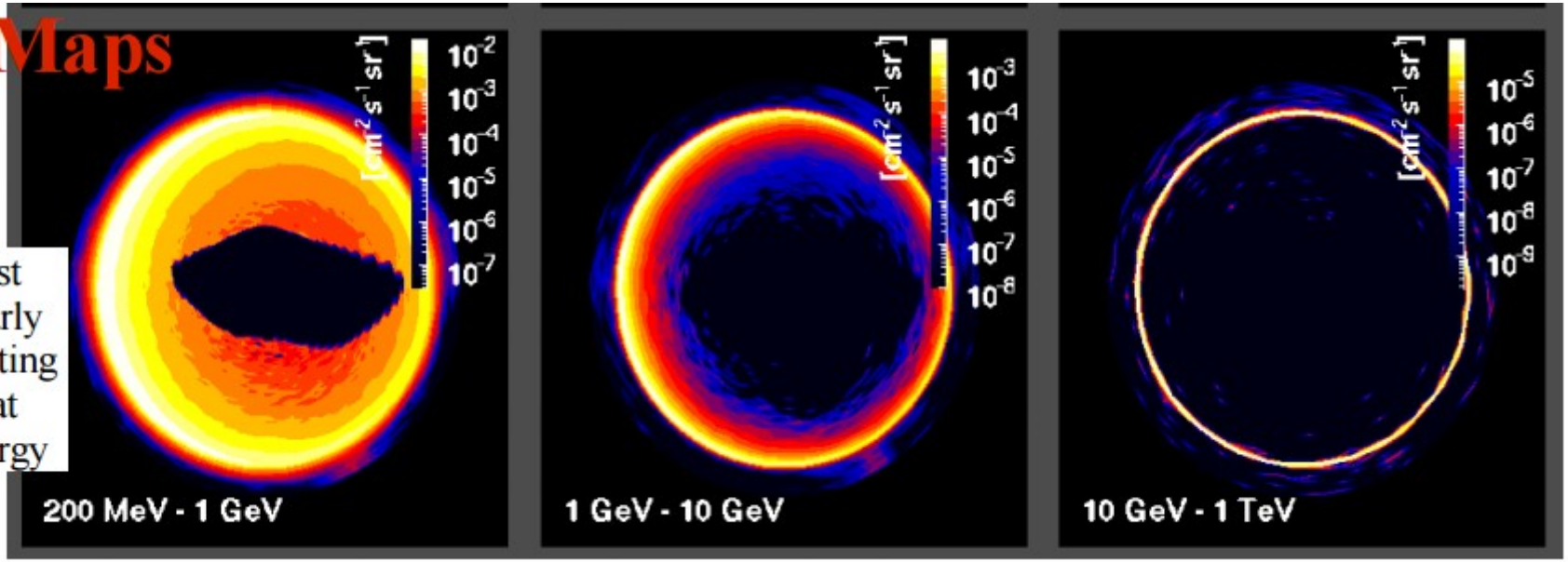

….and the Moon

2009 Fermi Symposium, Washington, D.C., Nov. 2-5

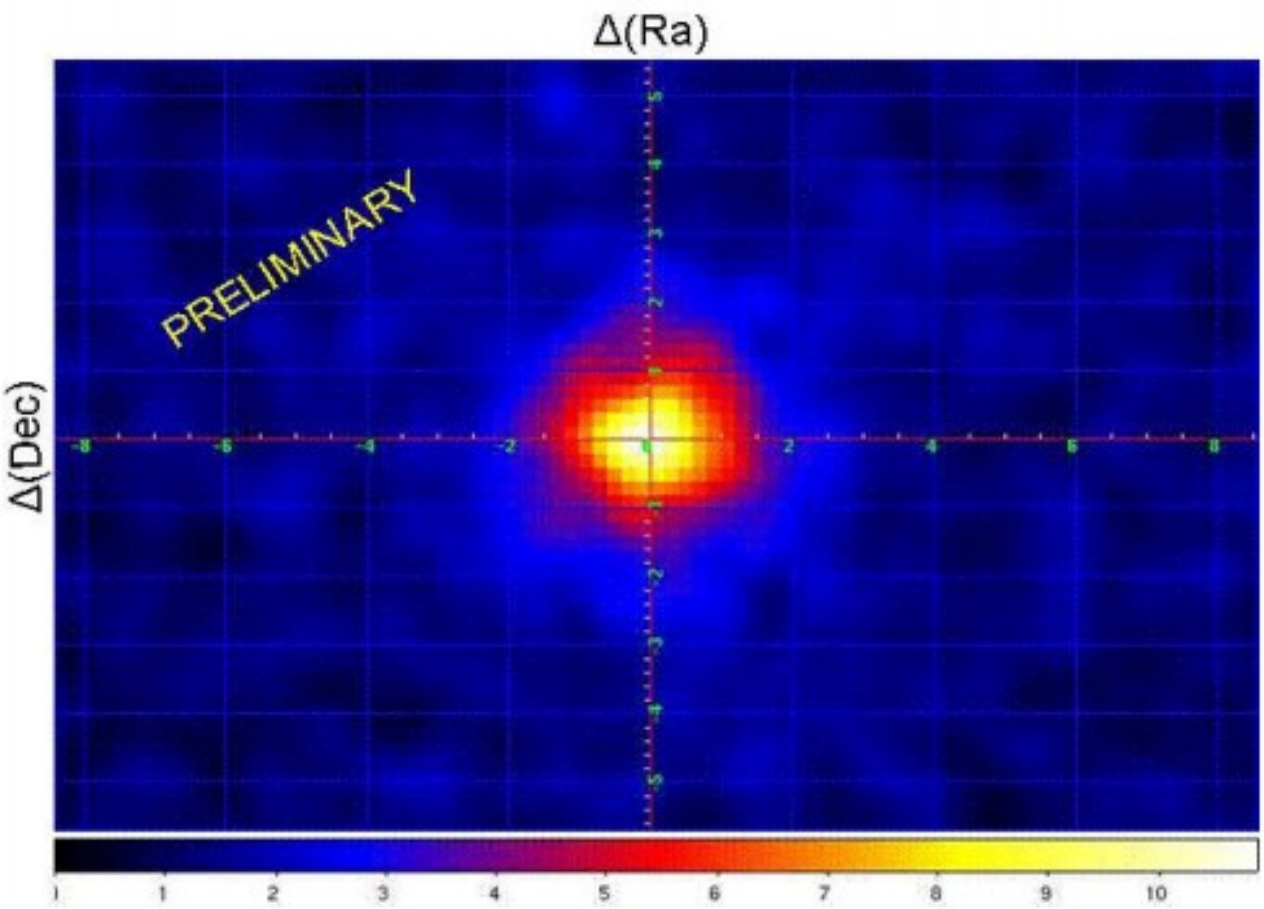

FIG. 1: Count map in a Moon centered frame, Right Ascension and Declination offsets in degrees respect to the Moon position in abscissa and ordinate respectively. The offset ranges are ± 8° for Right Ascension and ± 5° for Declination. The image has been obtained by using photons with E> 100 MeV, a bin width of 0.2 degrees with a gaussian smoothing 2 bin radius. The colour scale is linear with the counts.

Galactic diffuse gamma rays

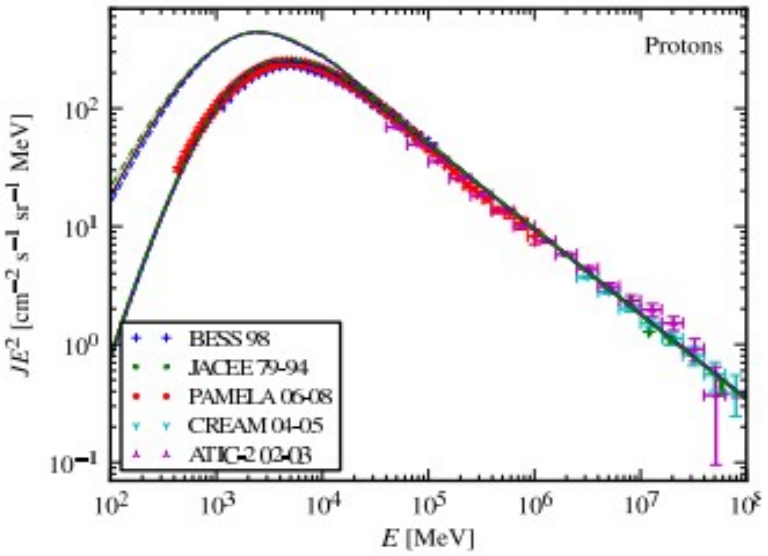

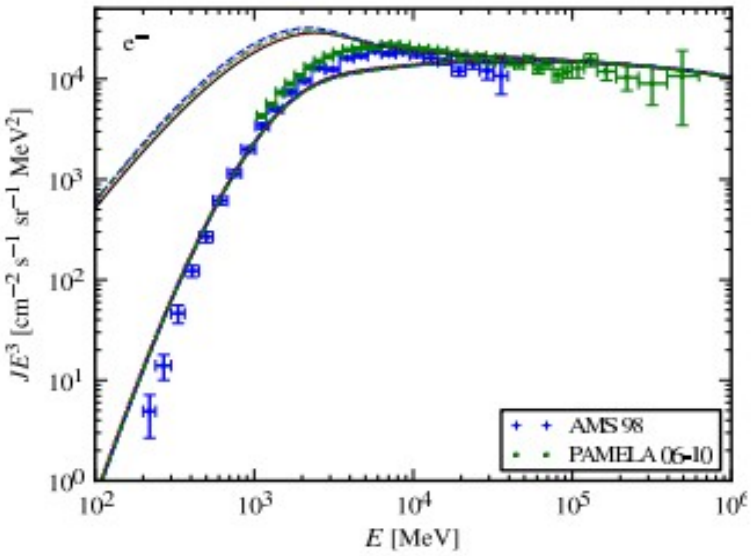

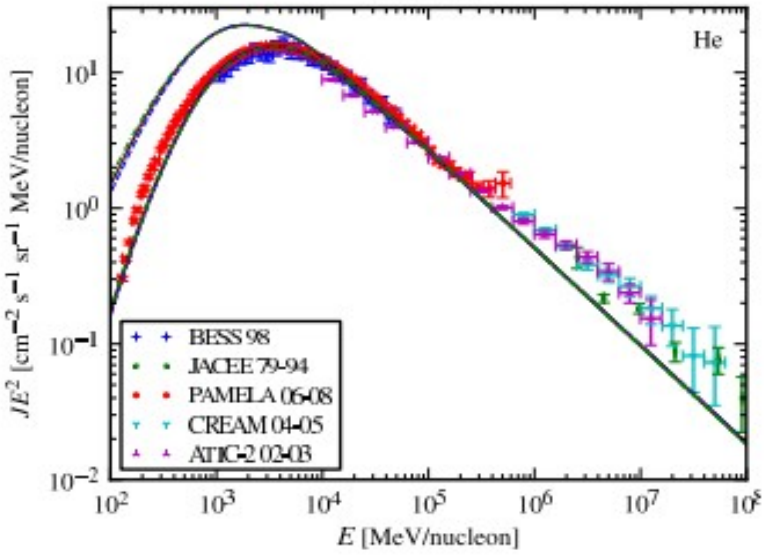

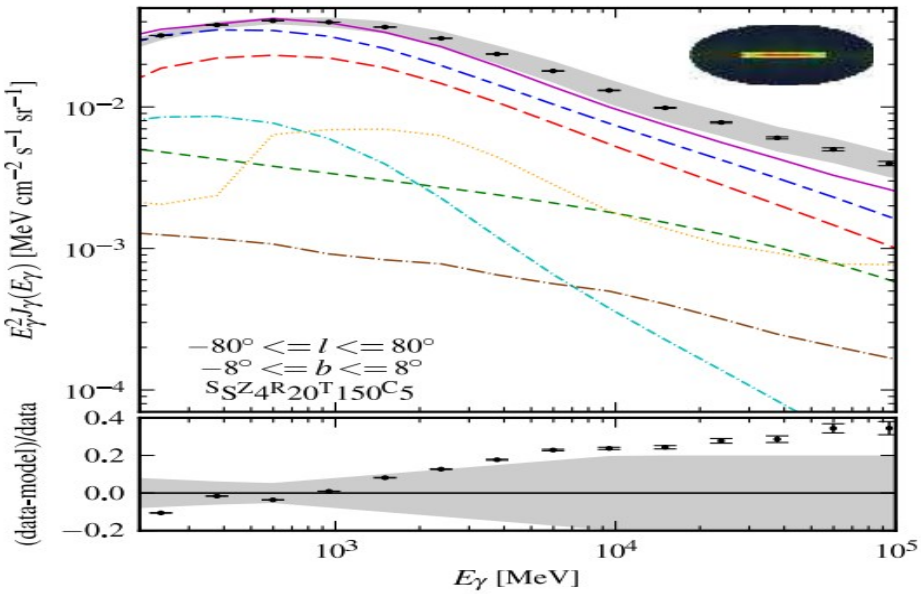

Fermi–LAT Observations of the Diffuse γ-ray Emission: Implications for Cosmic Rays and the Interstellar Medium

M. Ackermann[1], M. Ajello[2], W. B. Atwood[52], L. Baldini[3], J. Ballet[4], G. Barbiellini[5,6],

Galactic diffuse gamma rays

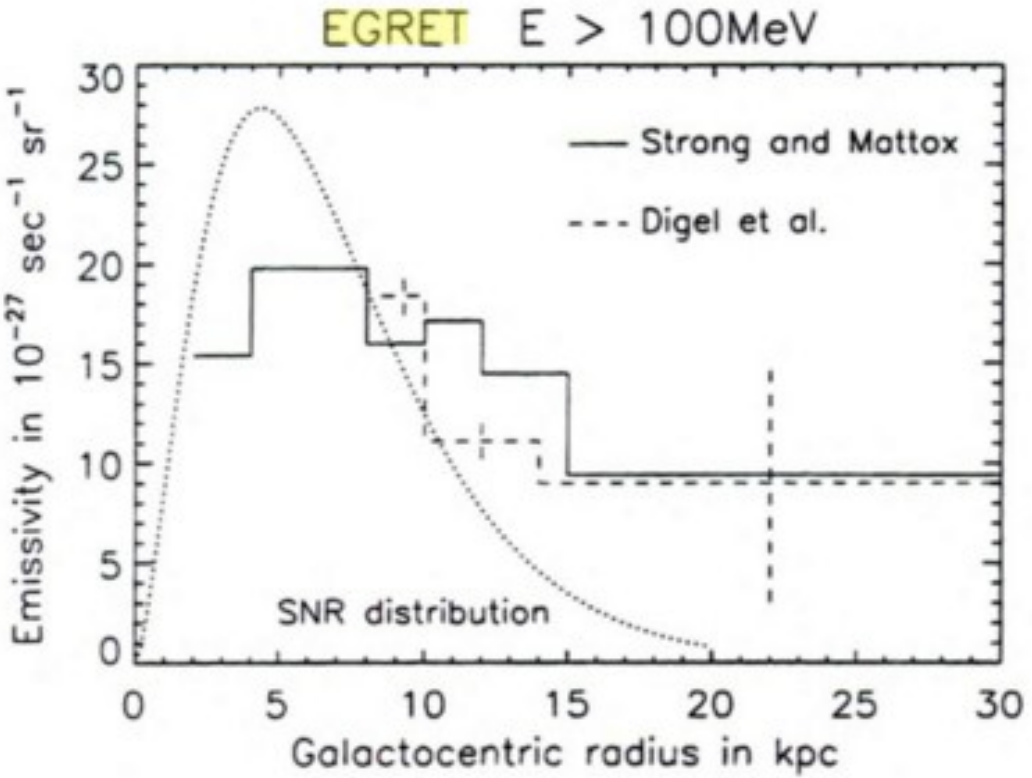

Fig. 6.10. A comparison between the γ-ray emissivity gradient (**solid histogram**) to the distribution of SNR as possible acceleration sites (**dotted line**). The statistical uncertainties of the gradient are typically below 10%. The obvious discrepancy implies that either SNR are not accelerating the bulk of GeV cosmic rays, or diffusive re-acceleration is operative, or galactic cosmic rays are confined on a scale of many kpc's. Note that locally derived emissivities (**dashed histogram**) can differ significantly from the global trend. From Strong and Mattox (1996 [528])

LMC diffuse gamma rays

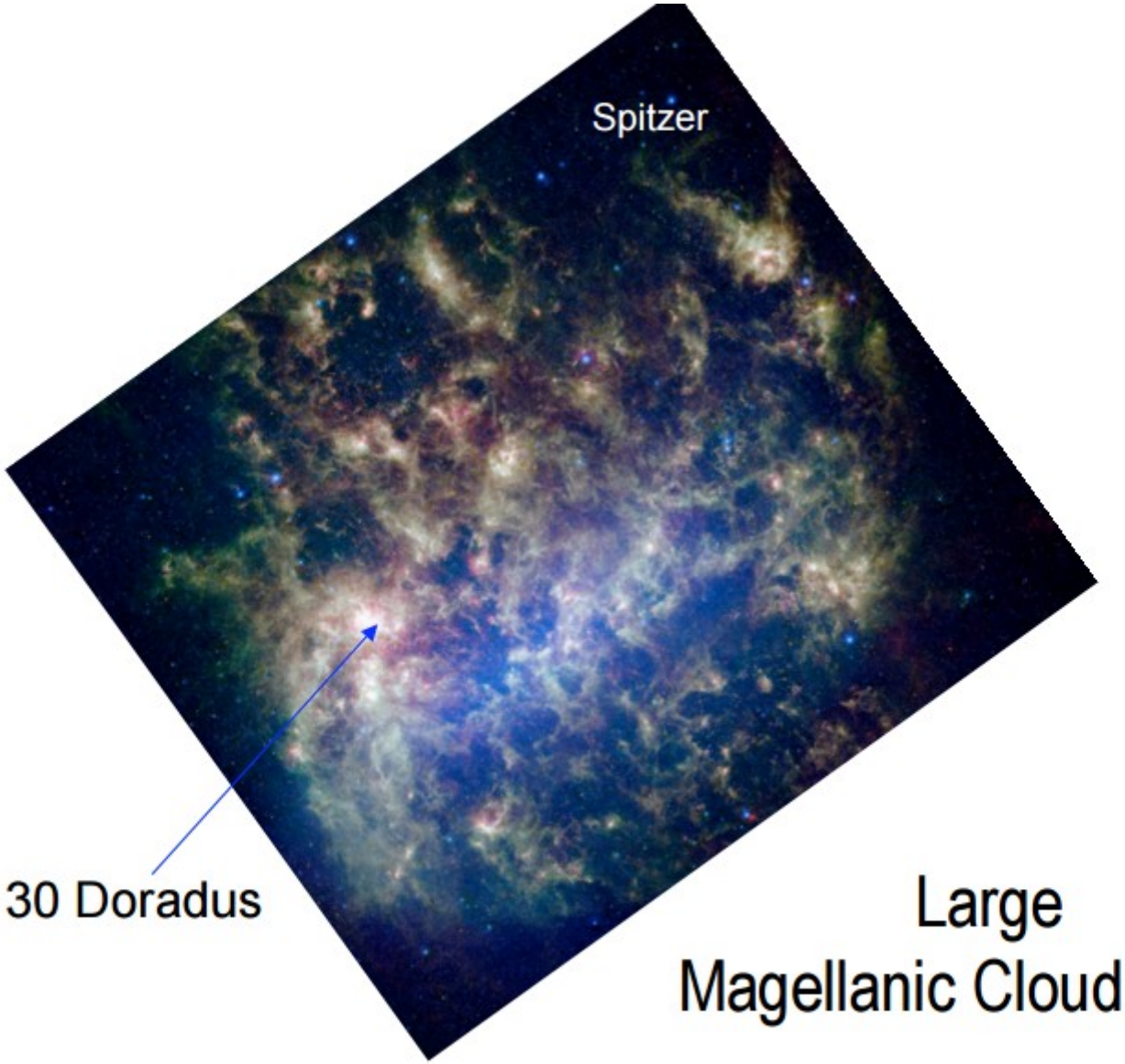

Large
Magellanic Cloud (LMC)

LMC diffuse gamma rays

LMC: counts maps 800MeV-8GeV and 8-80GeV (smoothing with gaussian of 0.2°)

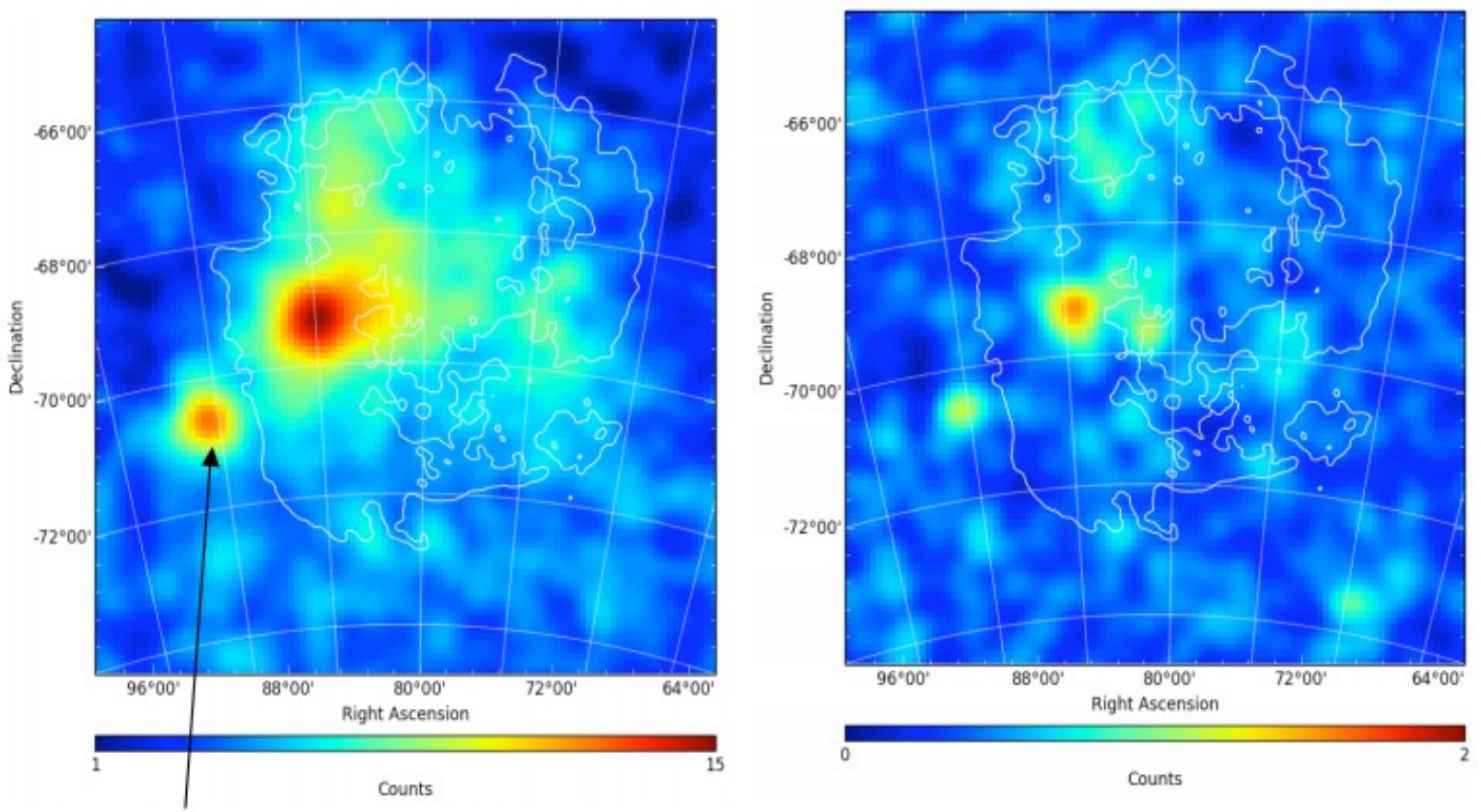

- A bright region, 30 Dor : what lies behind ?
- Extended emission not filling the galaxy or following the gas
- A few hard sources

LMC diffuse gamma rays

LMC: cosmic-ray population

An inhomogeneous distribution

- CR sea has 1/3 the local CR density
- CR enhancements by factors 2-8
- No CR enhancement in 30 Dor…
- … but >0.5° offset from it
- Correlation with cavities and shells

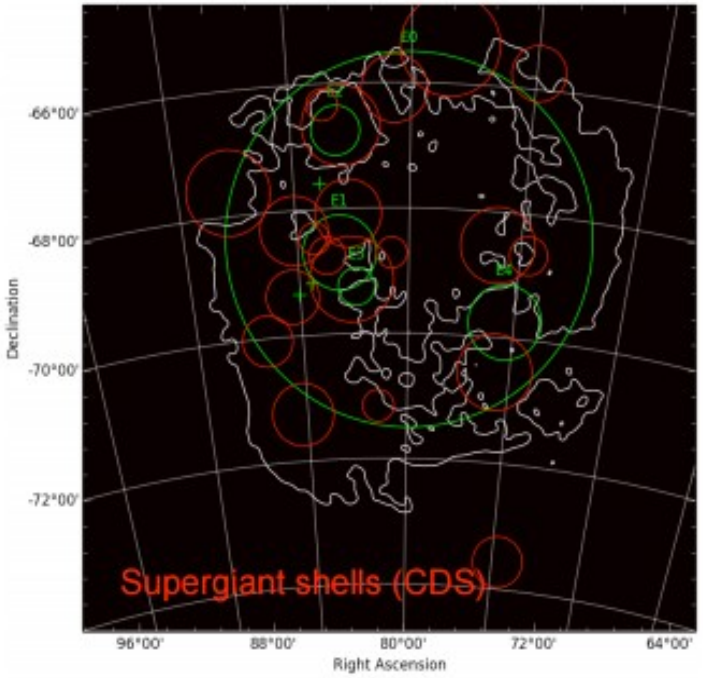

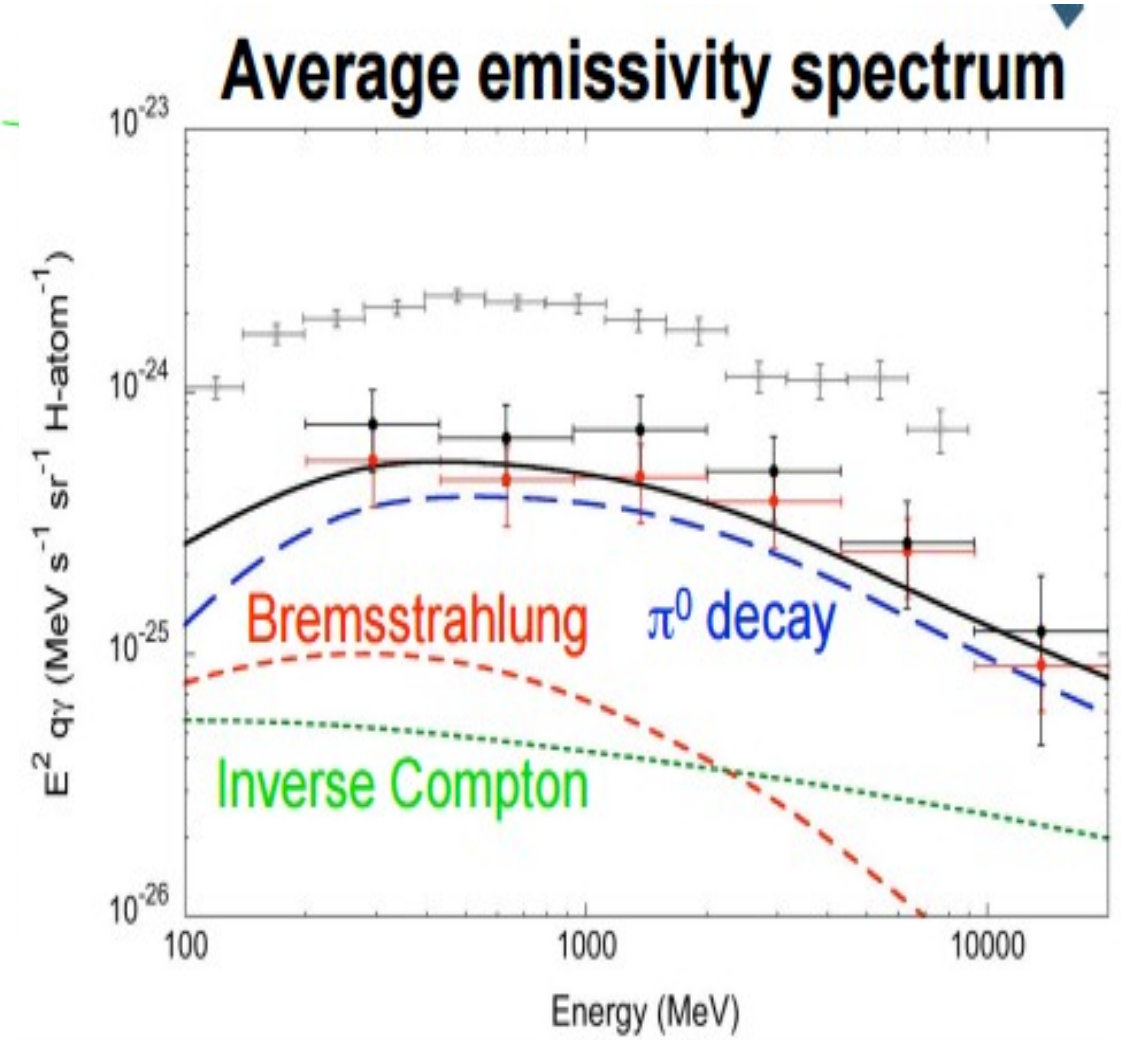

SMC diffuse gamma rays

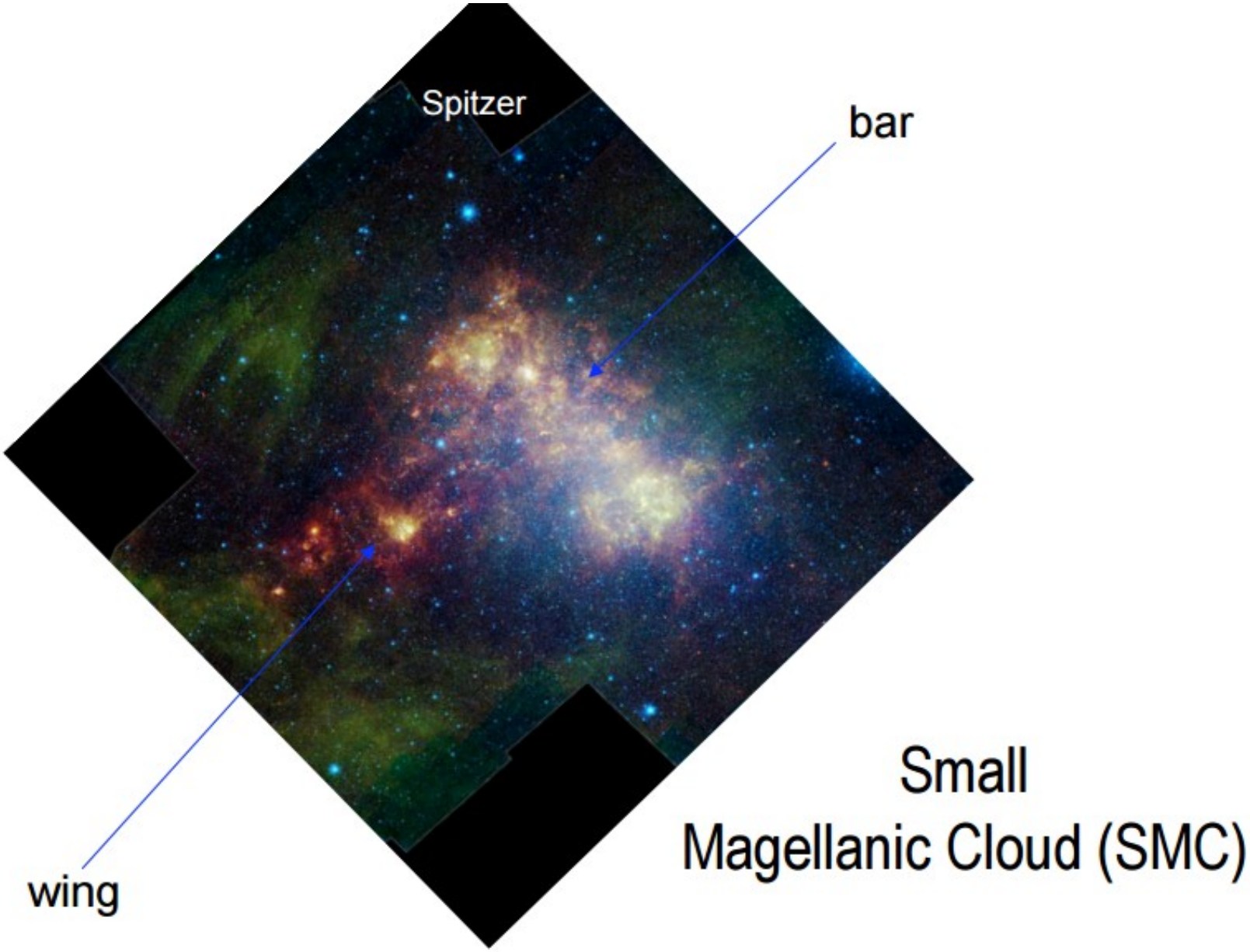

SMC diffuse gamma rays

SMC: counts maps 800MeV-8GeV and 8-80GeV (smoothing with gaussian of 0.2°)

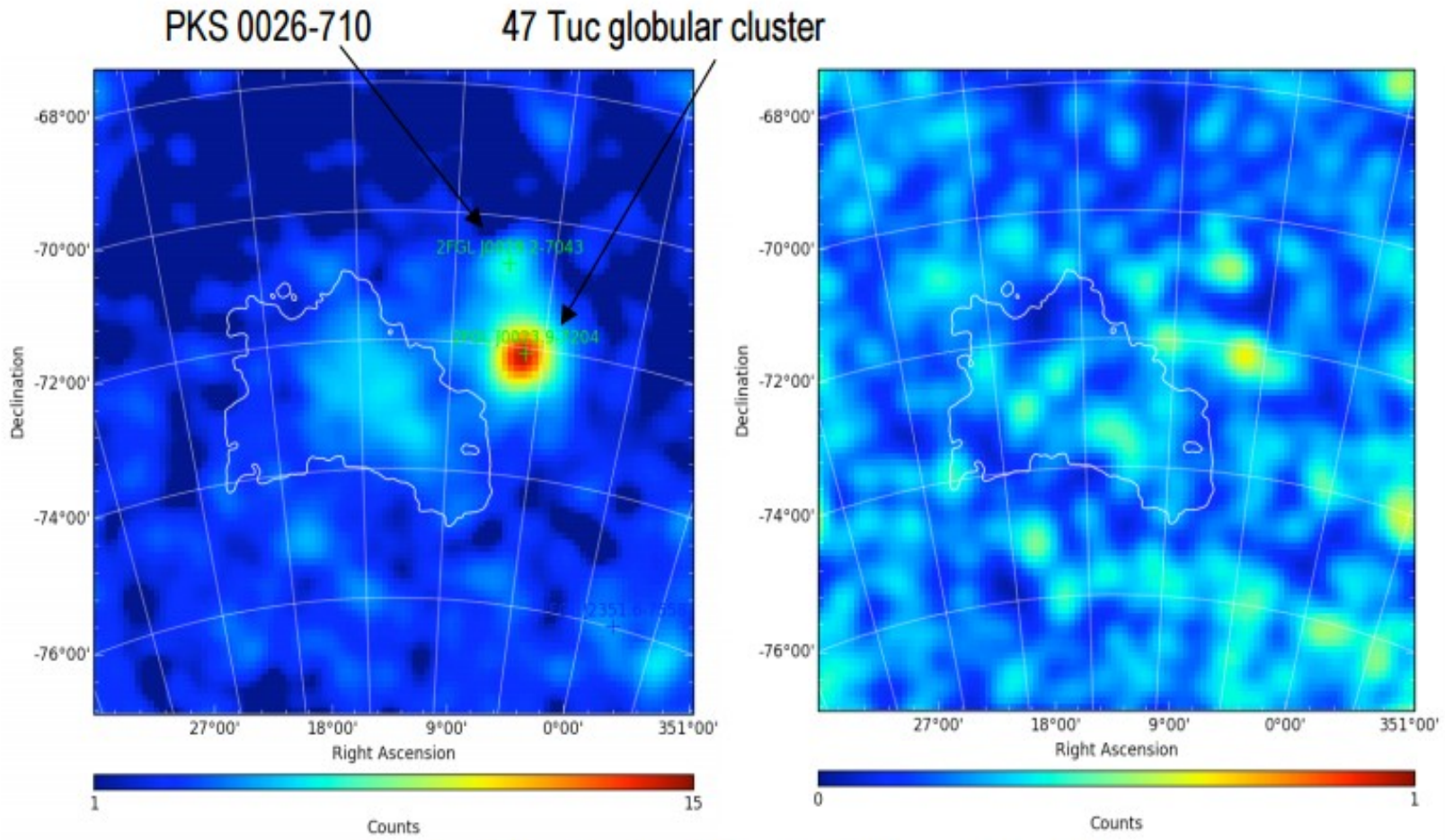

- Extended emission following the bar of the SMC
- No hard sources within SMC boundaries

SMC diffuse gamma rays

SMC: cosmic-ray population

Global picture differs from LMC

- No point-like source in SMC
- CR sea has ~5% the local CR density
- CR enhancement in the bar by ~4
- No obvious correlation with cavities

  …or star forming regions

  (but geometry is different)

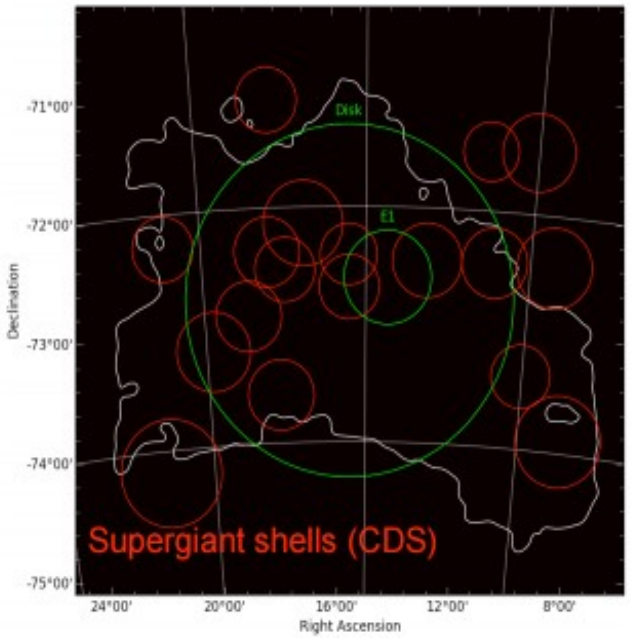

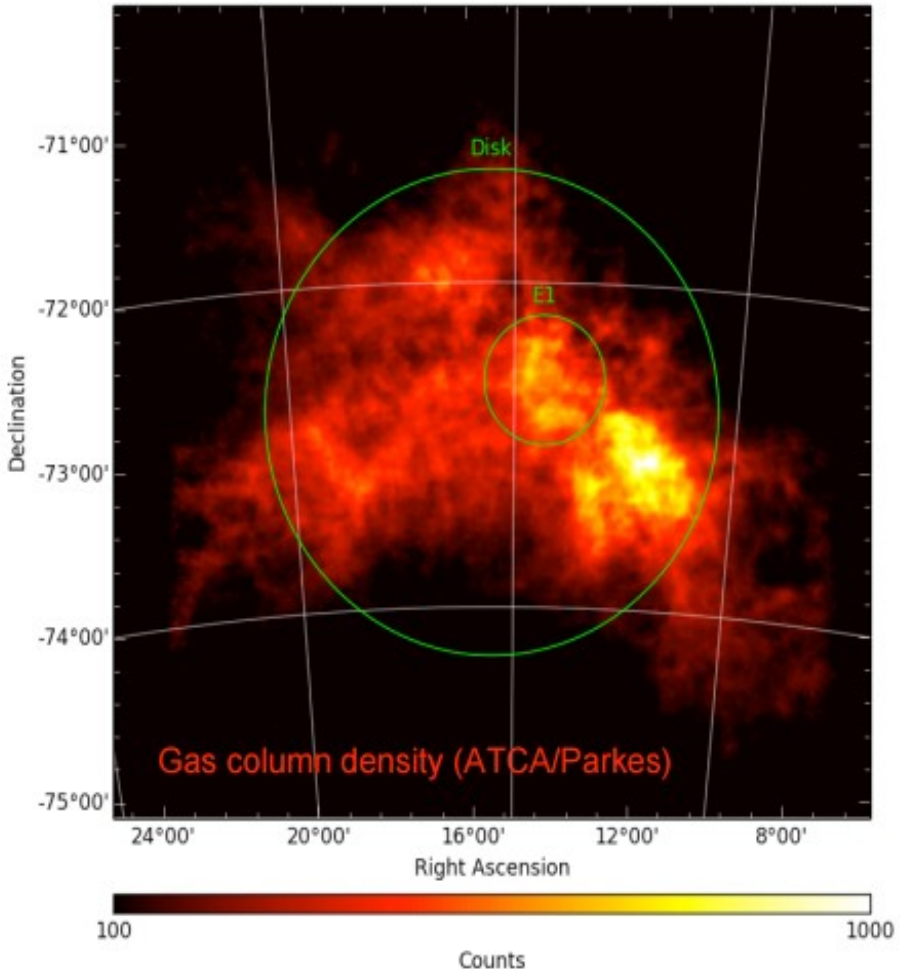

CR in other galaxies